Foulger Consulting

1025 Paradise Way
Palo Alto, CA 943062637, USA
Tel: 650/4932553
Cell: 650/9968886
FAX: 866/5326907
gillian@foulgerconsulting.com
http://www.foulgerconsulting.com/

November 12, 2014

WEEKLY REPORT #6 TO ALTAROCK ENERGY INC.

PROCESSING OF INDUCED EARTHQUAKES ASSOCIATED WITH THE NEWBERRY EGS INJECTION STARTING SEPTEMBER 2014

GILLIAN R. FOULGER & BRUCE R. JULIAN

Brief summary

During the last week, additional results were obtained for 10 more moment tensors. We are progressively deriving mechanisms for smaller events, but the quality of the results remains excellent in most cases. We added these additional events to our set of the highest-quality events for relative locations.

New results this week may be summarised:

1. *The addition of more, highly accurately measured and located earthquakes to the relative location set has revealed yet more fine detail. The pair of clusters identified earlier remains a stable feature, as does their clear separation by an essentially aseismic layer. The deeper cluster shows extraordinarily sharp focusing and appears to delineate an EW-trending plane and not a NW-trending plane as thought earlier. It appears to form part of the NW-trending zone observable in map view simply because it lies somewhat to the SE of the shallower cluster. The sharpness of the planar surface apparently delineated suggests that the relative locations may be accurate to a few meters, an unusually high-quality result. This interpretation also has support in the absolute locations which are suggestive of an EW orientation in the earthquakes of the deeper, more southerly cluster.*
2. *It is emphasised that relative location results will change with variation of run-time parameters and with the addition of more earthquakes to the set. The results described here appear to be stable as the run-time parameters are varied, but some changes may occur as the work progresses and the size of the dataset increases. The geometry of structures described here should thus be viewed as interim results.*
3. *The source types of the earthquakes for which moment tensors were derived continue to range from +Dipole to -Dipole.*
4. *A systematic variation in source type with time, during the three weeks of injection studied, is now visible in the growing data set. The proportion of crack-opening source types progressively reduces with time. During Week 1 about equal numbers of earthquakes were crack-opening and crack-closing types. The proportion of crack-opening events reduced to about 20% in Week 2 and in Week 3 none of the 9 moment tensors derived have a significant crack-opening component.*
5. *Variation in source-type with depth is also observed, with crack-opening source types more abundant and more extreme in the shallower cluster compared with the deeper cluster.*

The patterns of orientation of the P-, T- and I-axes reported earlier continue to strengthen in confidence with the addition of more data. Possible variations in orientations between the shallower and the deeper cluster were sought, but no evidence could be found. This suggests that the orientation of stress axes is similar in both hypocentral volumes.

1 Task 1 – Planning, conference calls, discussion of work, correspondence, followup

We continued to maintain contact with team members as before. The work continued to run on a routine basis.

2 Task 2 – System Setup

No additional system setup was done during the last week.

3 Task 3 – Quality control of prepicked MEQs and preparation for relocation and moment tensor calculation

We continued to derive moment tensors using the procedure described in our Weekly Report #1. We report here an additional 10 moment tensors, bringing the total number derived up to 54 (

Table 1). We have provided the locations and moment-tensor decomposition data of these new moment tensors to Trenton Cladouhos of AltaRock electronically, by email attachment.

Table 1: The 54 earthquakes for which moment tensors have been obtained to date. Locations given below are from the webpage http://fracture.lbl.gov/Newberry/locations.txt.

jday	month	day	hour	minute	sec	lat	lon	depth	magnitude
272	9	29	9	57	54.34	43.7245	-121.30857	0.845	0.721
272	9	29	18	3	37.724	43.72365	-121.30658	1.274	0.669
273	9	30	9	23	48.799	43.71965	-121.30908	0.854	0.853
273	9	30	21	30	43.689	43.72667	-121.313	0.387	0.972
274	10	1	1	3	14.64	43.7239	-121.30957	0.714	0.987
274	10	1	8	8	58.215	43.72623	-121.31412	1.196	0.848
274	10	1	10	50	55.229	43.72275	-121.30868	1.051	0.787
274	10	1	12	3	16.881	43.72658	-121.3158	1.587	1.086
274	10	1	15	1	55.056	43.72775	-121.31227	0.923	0.682
274	10	1	16	56	11.256	43.72232	-121.30712	1.65	0.901
275	10	2	6	38	47.428	43.7243	-121.31328	1.153	0.951
275	10	2	6	47	52.916	43.72632	-121.31322	1.323	1.117
275	10	2	12	39	9.082	43.7264	-121.31438	1.332	0.852
275	10	2	18	53	48.447	43.72082	-121.31372	1.671	0.957
275	10	2	20	36	50.997	43.72377	-121.31323	1.499	0.991

276	10	3	15	27	57.912	43.72257	−121.31562	1.054	0.919
276	10	3	18	54	54.199	43.72678	−121.31125	0.647	1.021
277	10	4	5	29	8.347	43.72578	−121.31068	0.946	0.922
278	10	5	2	6	17.079	43.7266	−121.31217	0.925	0.86
278	10	5	2	14	37.358	43.72433	−121.30915	0.459	0.665
278	10	5	15	55	21.373	43.73483	−121.30918	0.702	0.695
278	10	5	16	7	32.904	43.7253	−121.30967	1.205	0.819
278	10	5	23	22	16.638	43.72368	−121.3116	1.055	0.931
279	10	6	4	2	55.851	43.72307	−121.30835	0.835	0.637
279	10	6	6	13	48.787	43.72425	−121.3097	0.638	0.604
280	10	7	6	12	8.757	43.72372	−121.31015	0.564	0.791
280	10	7	10	47	21.079	43.72403	−121.3095	1.136	0.822
282	10	9	6	24	33.517	43.72232	−121.31203	0.735	0.769
282	10	9	10	16	9.958	43.7172	−121.31332	1.378	0.722
284	10	11	3	29	5.813	43.72417	−121.31338	0.409	0.852
284	10	11	10	53	26.568	43.72493	−121.30897	1.292	0.824
285	10	12	10	12	29.727	43.7257	−121.3135	0.783	0.863
285	10	12	16	47	1.174	43.7297	−121.3126	1.07	0.681
285	10	12	18	33	4.878	43.72363	−121.30787	0.359	0.743
285	10	12	21	10	18.995	43.72783	−121.31002	0.653	0.792
286	10	13	10	22	29.146	43.7302	−121.3153	0.831	0.907
287	10	14	5	46	14.161	43.71765	−121.31087	0.161	0.904
288	10	15	15	3	44.691	43.72658	−121.30768	0.897	0.781
288	10	15	15	37	26.034	43.72713	−121.30915	0.934	0.883
289	10	16	16	53	27.596	43.72378	−121.31295	−0.186	0.736
291	10	18	23	57	3.867	43.72965	−121.31732	0.116	0.781
292	10	19	9	7	50.375	43.73525	−121.3113	0.837	0.776
272	9	29	9	57	54.34	43.7245	−121.30857	0.845	0.721
272	9	29	18	3	37.724	43.72365	−121.30658	1.274	0.669
273	9	30	9	23	48.799	43.71965	−121.30908	0.854	0.853
273	9	30	21	30	43.689	43.72667	−121.313	0.387	0.972
274	10	1	1	3	14.64	43.7239	−121.30957	0.714	0.987
274	10	1	8	8	58.215	43.72623	−121.31412	1.196	0.848
274	10	1	10	50	55.229	43.72275	−121.30868	1.051	0.787
274	10	1	12	3	16.881	43.72658	−121.3158	1.587	1.086
274	10	1	15	1	55.056	43.72775	−121.31227	0.923	0.682
274	10	1	16	56	11.256	43.72232	−121.30712	1.65	0.901
275	10	2	6	38	47.428	43.7243	−121.31328	1.153	0.951
275	10	2	6	47	52.916	43.72632	−121.31322	1.323	1.117

4 Task 4 –Improved locations and relative locations

4.1 Absolute locations

We have updated our map of events for which moment tensors were derived and the full 54-event dataset is shown in Figure 1 and Figure 2.

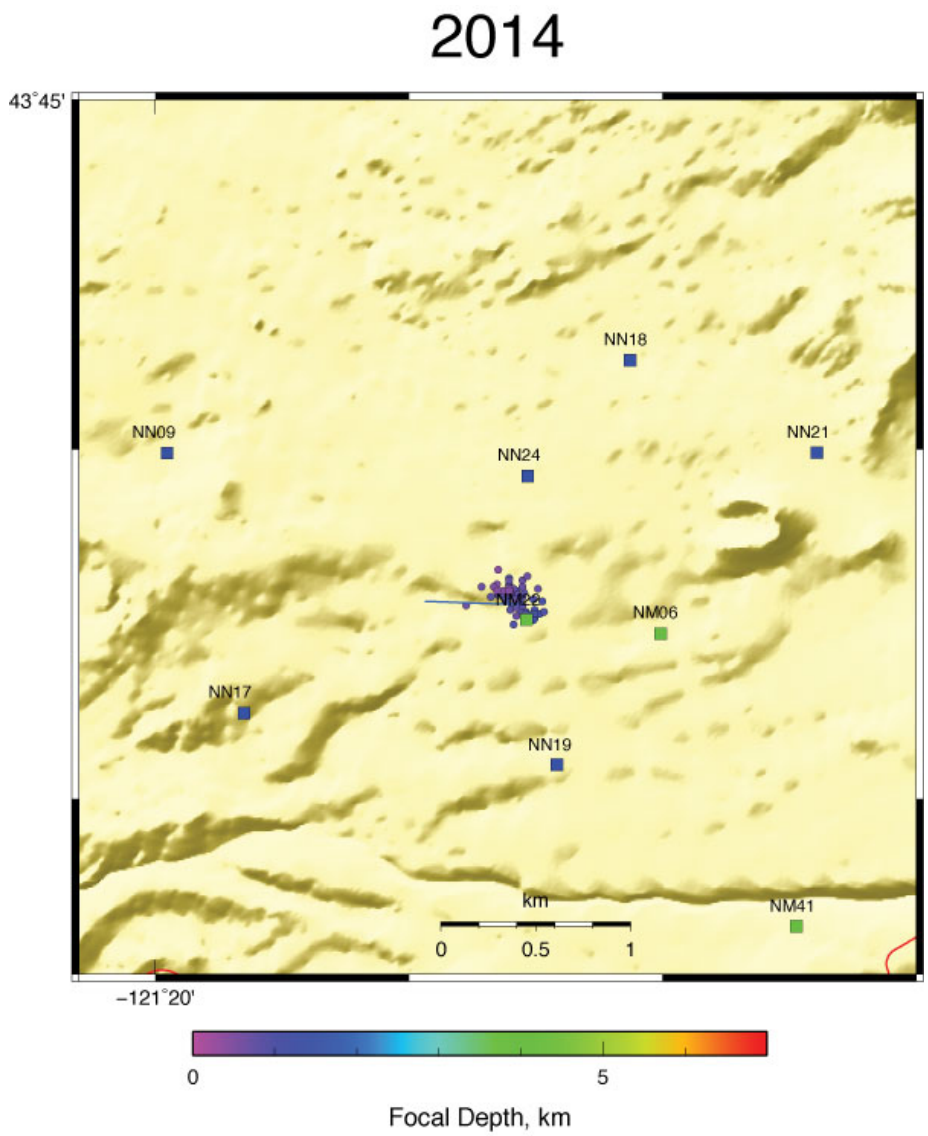

Figure 1: High quality estimated hypocenters of 54 microearthquakes that occurred between Sept. 29 and Oct. 19, 2014, and for which moment tensors were derived. These locations are computed using

arrival times measured carefully in connection with the moment-tensor analysis. Well NWD 55-29 is shown in blue.

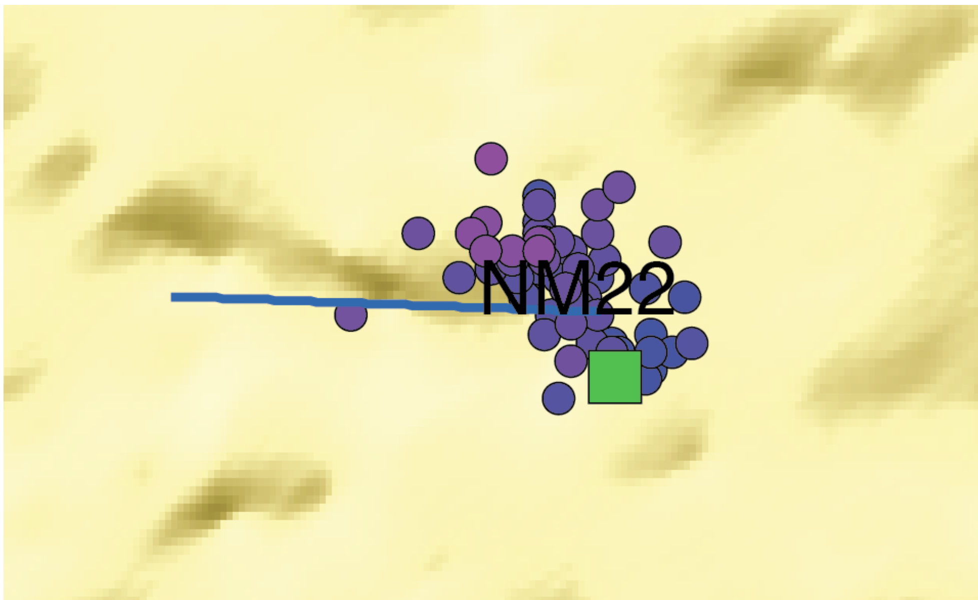

Figure 2: Expanded view of the locations of the earthquakes for which moment tensors were derived.

4.2 Relative locations

We continued with the relative location work, applying the method to the 54 earthquakes for which moment tensors have now been derived. These events are the best-located set currently available. We used the same procedure as described in earlier reports.

We explored further different run-time parameters. Different parameters are optimal for different data sets so this must be done each time a new dataset is subject to relative location. We performed about 12 trial inversions and found the following to give the best result. This is the result that shows in the most focus, patterns in the results which appear to be stable across several sets of results obtained using different run-time parameter choices.

- *minclust*–the minimum number of earthquakes to define a cluster (a value of 8 was used);
- *maxit*–the maximum allowed number of relocation iterations (optimal value identified = 7);
- *maxsep*–the maximum separation allowed between linked pairs of earthquakes (optimal value identified = 0.15 km);
- *minlinks*–the minimum number of “links” (i.e., measured station/phases in common between pairs of earthquakes) needed for an earthquake to be passed to the final relocated set (optimal values identified = 21);

This inversion read in the 54 original earthquakes. 25 failed the *minlinks* cut-off criterion, and a further 5 failed the *maxsep* criterion. This left the 24 highest-quality earthquakes, which fell into two clusters, one containing 16 earthquakes (the shallower cluster) and the other 8 earthquakes (the deeper cluster).

The two clusters were fixed by pinnning them to one excellently located earthquake in each cluster (i.e., a total of two earthquakes). The following were used:

- `2014 10 01 14 53 20.145 43.726509 -121.309105 0.82 0.0 0.00 0.00 0.0 11`
- `2014 10 01 08 08 57.998 43.725528 -121.308941 1.21 0.0 0.00 0.00 0.0 6`

The results are shown in Figure 3 to Figure 6.

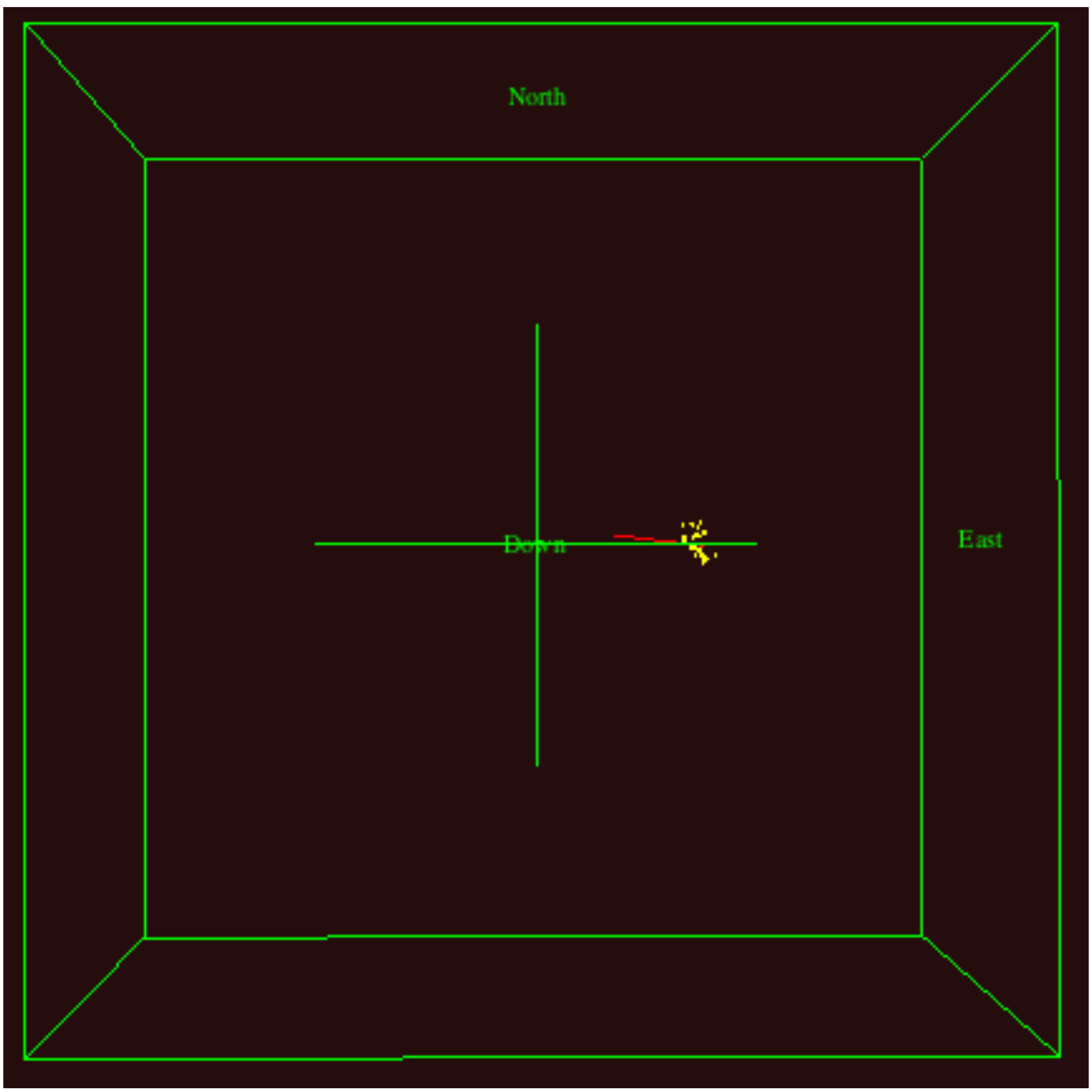

Figure 3: Map of relative locations of 24 moment-tensor earthquakes that occurred in the time period 29 September - 19 October, 2014. Runtime parameters used were *minclust* = 8, *maxit* = 7, *maxsep* = 0.15 km, *minlinks* = 21.

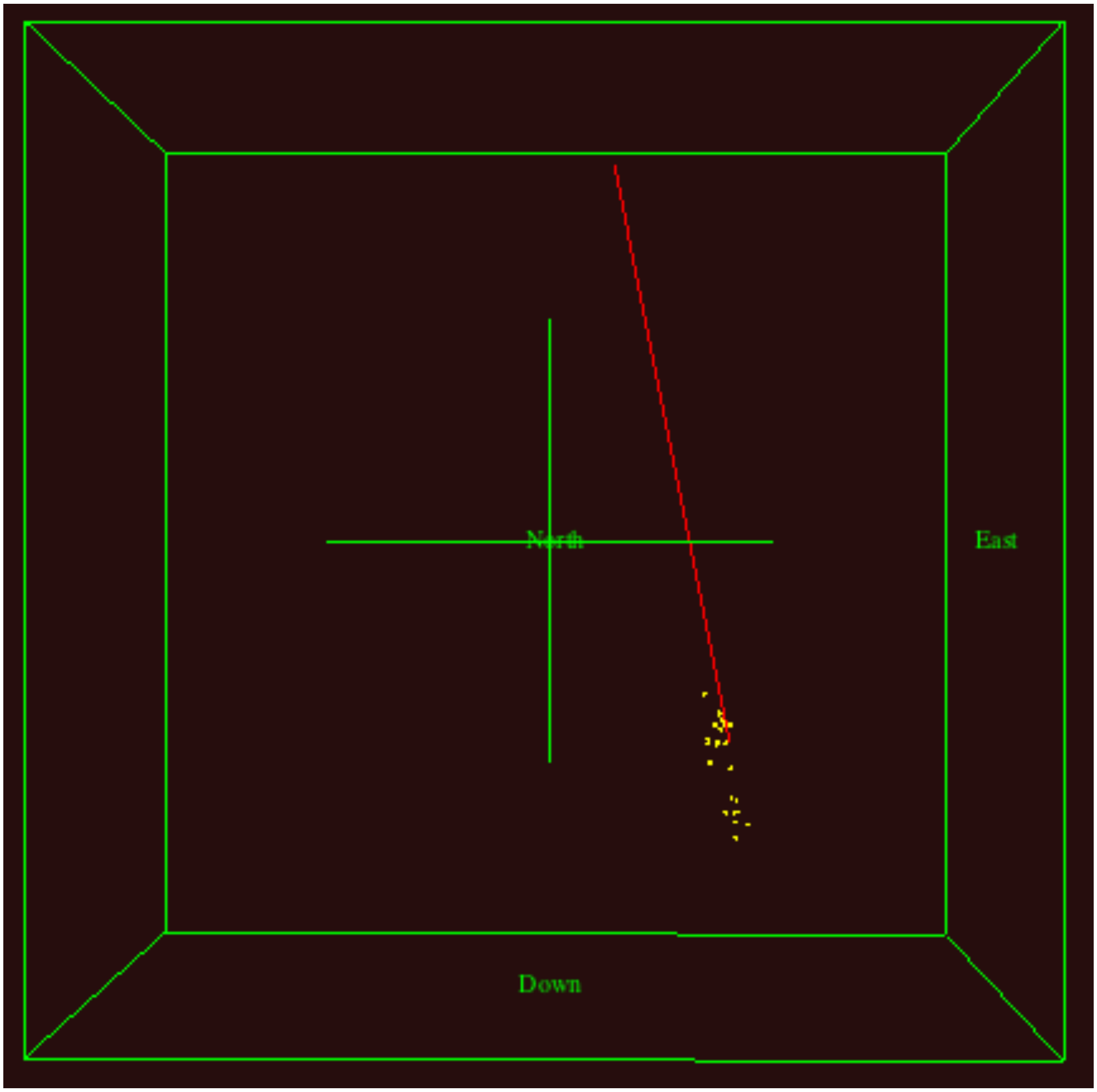

Figure 4: Same as Figure 3 except in cross section looking north.

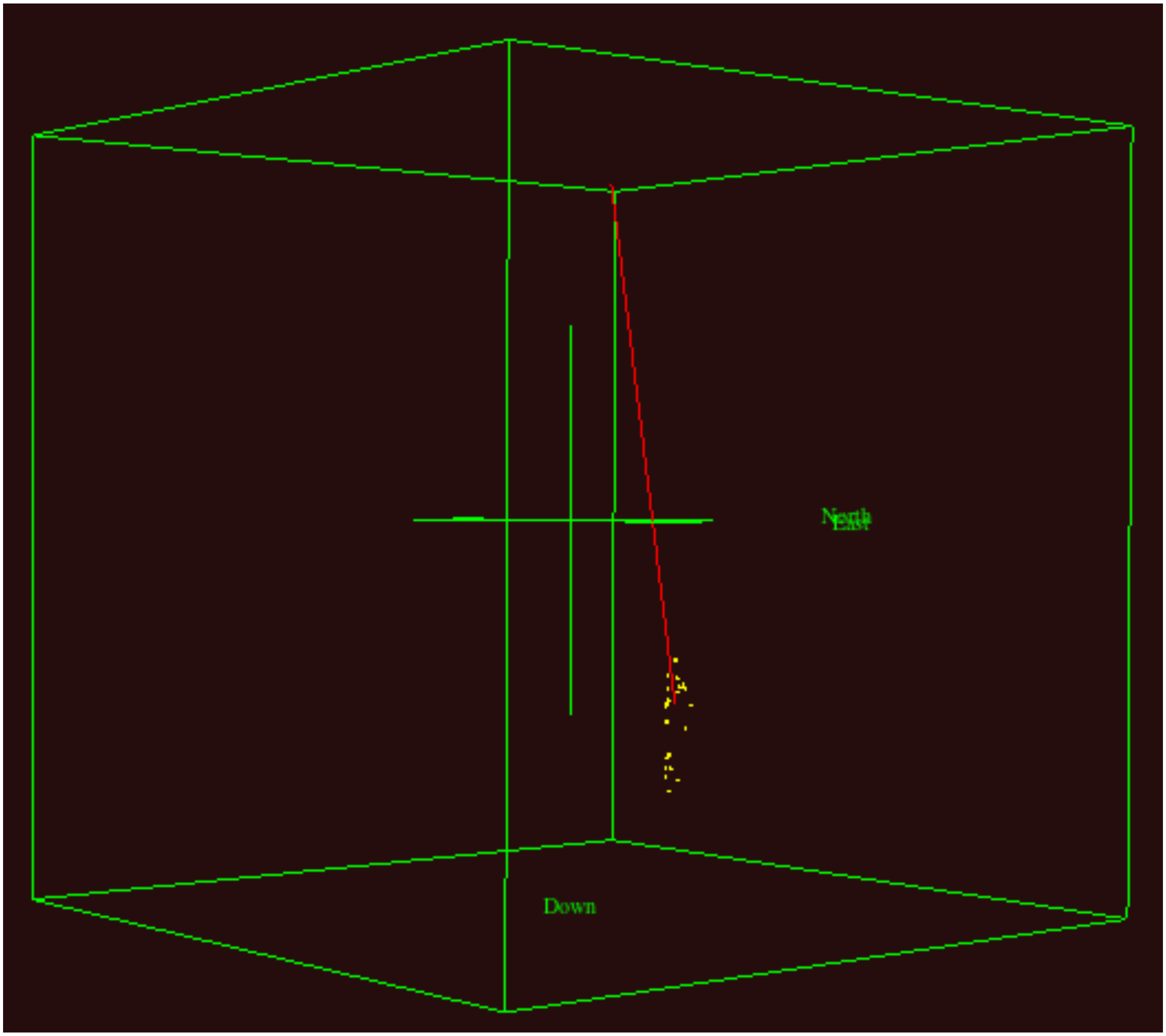

Figure 5: Same as Figure 3 except in cross section looking northwesterly, along the strike of the planar structure visible in map view.

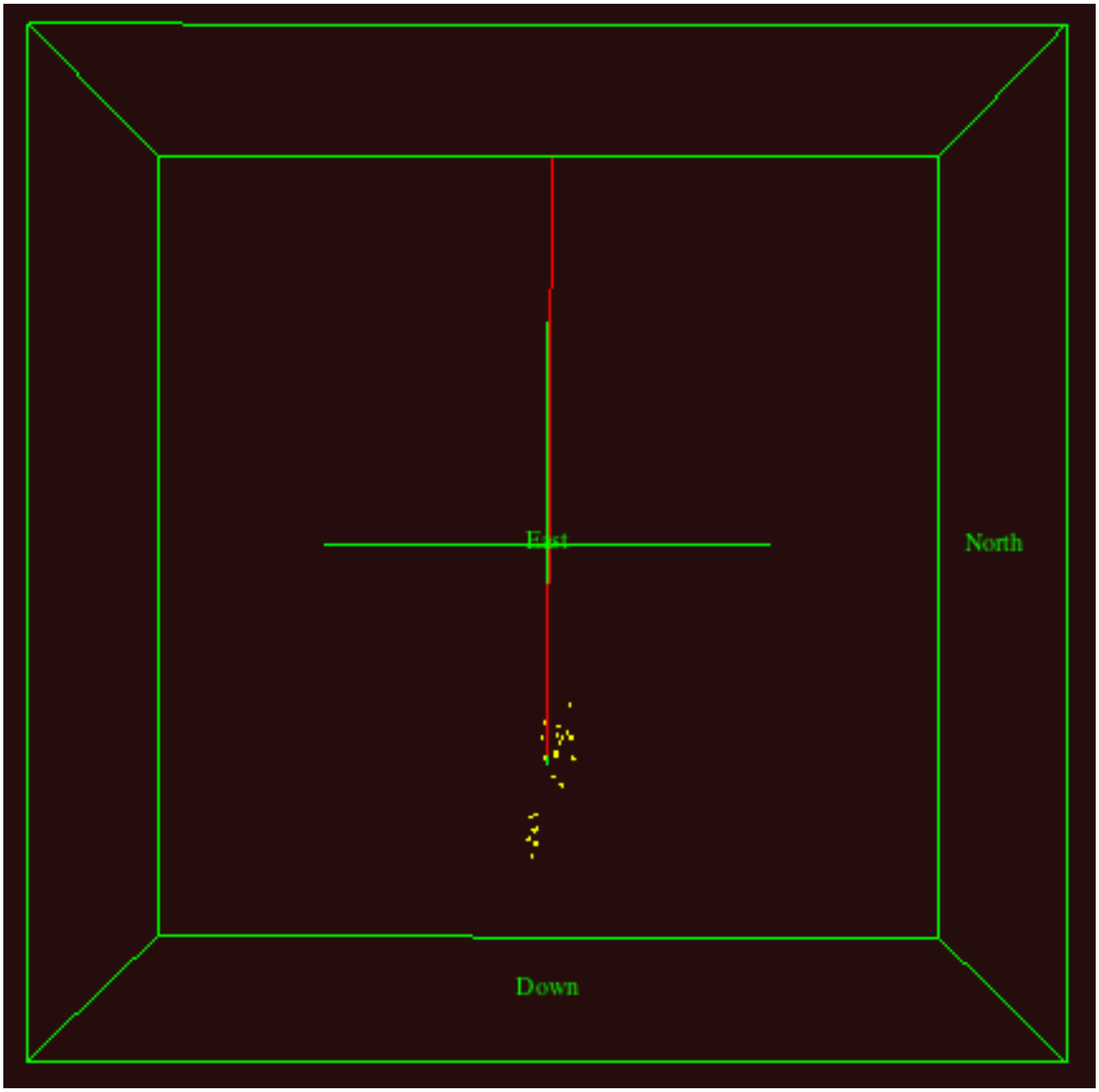

Figure 6: Same as Figure 3 except in cross section looking easterly.

The relative location results continue to reveal intriguing new patterns. The results described in earlier reports are confirmed, but with increasing detail suggested. In map view (Figure 3) the epicenters delineate clear linear zone striking at ~ N 45˚W. In cross section, two separate clusters are visible, separated by a depth interval ~ 200 m thick with very few earthquakes.

A cross section looking northwesterly along the strike of the surface trend (Figure 5) shows a more focused picture, with the earthquakes presenting a much narrower aspect. However, in a cross section looking due west, the lower cluster appears to be even more focused. It shows extremely sharp edges suggesting that relative locations may be accurate even to a few meters. Further investigation of this is warrented, along with a concentrated effort to process as many of the larger earthquakes as possible in order to increase the size of this excellent subset of locations.

The relocated hypocenters were studied at some length, rotating the plot in three dimensions using the *Mathematica* software There is a suggestion that the lower cluster may occur on an EW orientated planar structure, and not on a NW-orientated one. It may be that it forms just the southeasternmost part of the NW-elongated epicentral trend observed in map view (Figure 1, Figure 2 and Figure 3) but does not itself lie on a structure with this trend. In fact, the distribution of epicenters shown in Figure 2 also suggests this, with a remarkably sharp linear array of earthquakes visible south of Well NWD 55-29.

Numerical data for these interim results have been provided to AltaRock by email attachment to Trenton Cladouhos.

5 Task 5 Moment tensor calculations

The numerical results of the entire moment-tensor catalog, including the 10 new results obtained during the last week, are given in Appendix 1. Graphical results for the additional 10 events are given in Appendix 2.

The source types for the entire 54-event set are shown in source-type space in Figure 7. The distribution remains similar to that reported earlier, i.e., source types ranging from +Dipole to -Dipole.

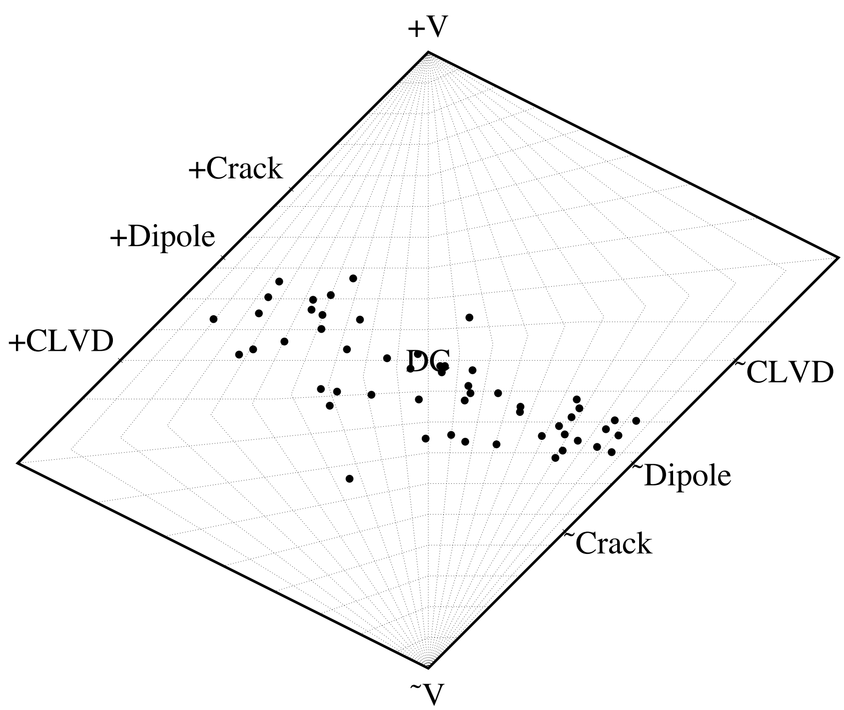

Figure 7: Source-type plot showing the 54 earthquakes for which moment tensors have been derived to date.

The data set is now large enough that temporal variations in source type can be studied. Figure 8 shows source-type plots for Week 1 of the stimulation (29 September -5 October), Week 2 (6-13 October), and Week 3 (14-20 October). A systematic variation in source type is evident, with the proportion of crack-opening source types progressively reducing. During Week 1 about equal numbers were crack-opening and crack-closing types. The proportion of crack-opening events reduced to about 20% in Week 2 and in Week 3 none of the 9 moment tensors derived have a significant crack-opening component.

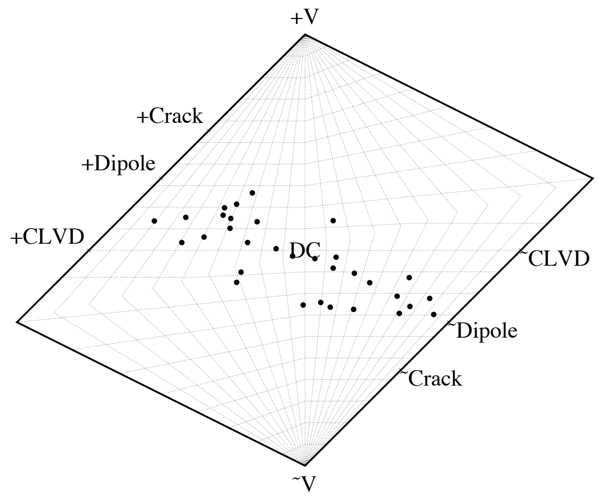
+V
+Crack
+Dipole
+CLVD
DC
~CLVD
~Dipole
~Crack
~V

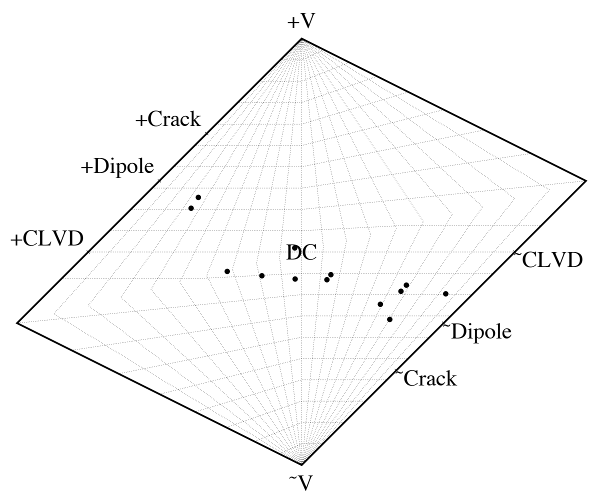
+V
+Crack
+Dipole
+CLVD
DC
~CLVD
~Dipole
~Crack
~V

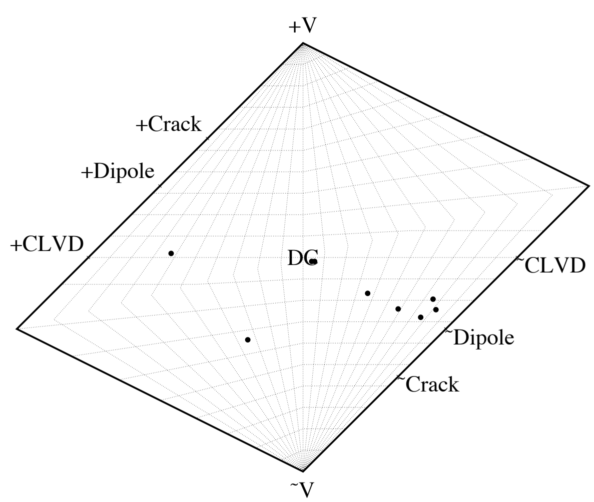
+V
+Crack
+Dipole
+CLVD
DC
~CLVD
~Dipole
~Crack
~V

Figure 8: Top: Moment tensors for Week 1 of the stimulation (29 September -5 October), Middle: Moment tensors for Week 2 of the stimulation (6-13 October), Bottom: Moment tensors for Week 3 of the stimulation (14-20 October).

Figure 9 shows the source types divided up by depth. The upper panel shows source types in the shallower group of earthquakes observed in the relative locations (e.g., Figure 6), and the lower panel shows events in the deeper group. Both sets of earthquakes have source types that extend almost to the -Dipole point (crack closing) but the shallower group has more sources close to the +Dipole point, indicating crack opening. These extreme crack-opening source types are both more numerous and more extreme in the shallower event group.

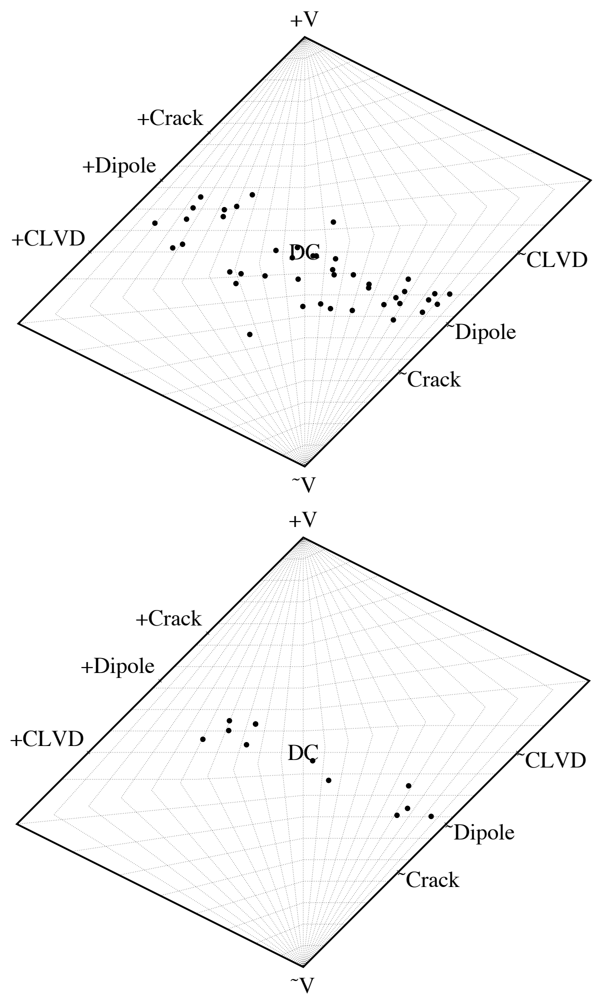

Figure 9: Top: Source types of earthquakes shallower than 1 km b.s.l., Bottom: Source types of earthquakes deeper than 1 km b.s.l.

Figure 10 shows a plot of the P-, T- and I-axes, approximately corresponding to the directions of σ_1, σ_3 and σ_2. The addition of more earthquakes has strengthened the distribution seen earlier. Most T axes cluster systematically subhorizontally and to the S ± 20˚ or so. The orientations of the P-axes show some clustering in a sub-horizontal orientation to the NNE-ENE directions.

Figure 11 shows P-, T-, and I-axes for the earthquakes that located deeper than 1 km only, i.e. events in the lower group identified in the relative locations. The distribution is similar, overall, to the events as a whole. This suggests that there is no evidence in the moment-tensor dataset obtained to date for a rotation of the stress axes with depth in the stimulated volume.

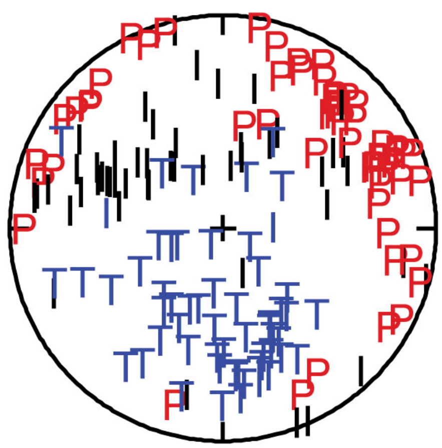

Figure 10: Plot of pressure (P ~ σ_1) and tension (T ~ σ_3) and intermediate (I ~ σ_2) axes for the 44 earthquakes for which moment tensors have been derived to date.

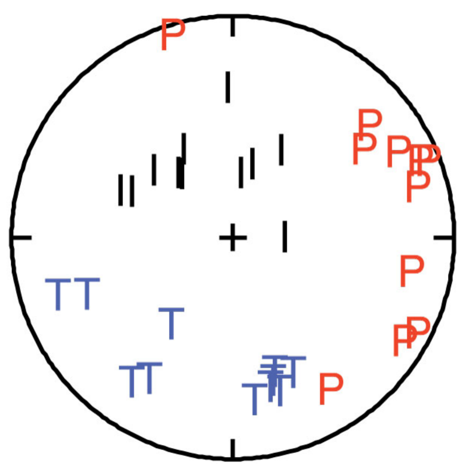

Figure 11: Plot of pressure (P ~ σ_1) and tension (T ~ σ_3) and intermediate (I ~ σ_2) axes for the 11 earthquakes for which moment tensors have been derived that were located deeper than 1 km depth.

6 Brief summary statement

During the last week, additional results were obtained for 10 more moment tensors. We are progressively deriving mechanisms for smaller events, but the quality of the results remains excellent in most cases. We added these additional events to our set of the highest-quality events for relative locations.

New results this week may be summarised:

6. The addition of more, highly accurately measured and located earthquakes to the relative location set has revealed yet more fine detail. The pair of clusters identified earlier remains a stable feature, as does their clear separation by an essentially aseismic layer. The deeper cluster shows extraordinarily sharp focusing and appears to delineate an EW-trending plane and not a NW-trending plane as thought earlier. It appears to form part of the NW-trending zone observable in map view simply because it lies somewhat to the SE of the shallower cluster. The sharpness of the planar surface apparently delineated suggests that the relative locations may be accurate to a few meters, an unusually high-quality result. This interpretation also has support in the absolute locations which are suggestive of an EW orientation in the earthquakes of the deeper, more southerly cluster.
7. It is emphasised that relative location results will change with variation of run-time parameters and with the addition of more earthquakes to the set. The results described here appear to be stable as the run-time parameters are varied, but some changes may occur as the work progresses and the size of the dataset increases. The geometry of structures described here should thus be viewed as interim results.
8. The source types of the earthquakes for which moment tensors were derived continue to range from +Dipole to -Dipole.
9. A systematic variation in source type with time, during the three weeks of injection studied, is now visible in the growing data set. The proportion of crack-opening source types progressively reduces with time. During Week 1 about equal numbers of earthquakes were crack-opening and crack-closing types. The proportion of crack-opening events reduced to about 20% in Week 2 and in Week 3 none of the 9 moment tensors derived have a significant crack-opening component.
10. Variation in source-type with depth is also observed, with crack-opening source types more abundant and more extreme in the shallower cluster compared with the deeper cluster.
11. The patterns of orientation of the P-, T- and I-axes reported earlier continue to strengthen in confidence with the addition of more data. Possible variations in orientations between the shallower and the deeper cluster were sought, but no evidence could be found. This suggests that the orientation of stress axes is similar in both hypocentral volumes.

Appendix 1: Numerical moment tensor results for the 54 MEQs studied to date. N=North, E=East, D=Down.

NN	NE	EE	ND	ED	DD	Year	Mo	Day	Hr	min	Sec	Quality
1.578e-01	3.466e-02	6.671e-02	2.482e-01	6.317e-02	8.338e-02	2014	10	01	14	53	05.23	excellent
2.172e-01	-3.673e-02	-6.417e-02	2.346e-01	7.204e-02	3.184e-02	2014	10	01	19	05	16.54	excellent
8.713e-02	1.262e-01	-4.193e-02	1.814e-01	8.429e-02	8.722e-02	2014	10	04	18	51	12.00	excellent
-1.029e-01	1.325e-01	-1.185e-01	1.480e-01	5.508e-02	1.074e-01	2014	10	04	17	32	52.76	excellent
-1.165e-01	1.705e-01	-1.989e-01	1.394e-01	-2.430e-02	1.639e-02	2014	10	02	07	07	04.16	excellent
2.406e-01	-7.298e-02	-9.789e-02	1.731e-01	4.297e-02	8.349e-02	2014	10	02	11	01	42.38	excellent
-1.461e-02	9.643e-02	-3.978e-01	2.595e-02	1.691e-01	-4.693e-03	2014	10	02	06	47	52.94	excellent
6.066e-03	-2.231e-01	-9.157e-02	1.941e-01	3.367e-02	-6.184e-04	2014	10	03	06	06	22.76	excellent
-5.772e-02	-1.655e-01	-1.427e-01	1.464e-01	7.811e-02	-1.952e-02	2014	10	03	18	54	53.93	fair
2.004e-01	-1.410e-01	-1.461e-01	1.400e-01	-8.713e-03	7.412e-02	2014	10	01	12	03	16.94	good
5.304e-02	6.783e-02	-1.175e-01	1.615e-01	7.508e-02	2.206e-01	2014	10	05	04	07	20	excellent
-1.777e-01	-1.053e-01	-1.512e-01	7.111e-02	1.063e-01	1.057e-01	2014	10	01	01	03	14.49	excellent
-2.667e-01	1.320e-01	-6.399e-02	6.063e-02	1.031e-01	7.787e-02	2014	09	30	21	30	43.503	excellent
-1.871e-01	8.995e-02	-9.473e-02	-1.446e-01	-2.491e-02	1.992e-01	2014	10	05	23	22	16.499	good
1.684e-01	-3.350e-02	-9.826e-03	2.952e-01	3.542e-02	9.350e-02	2014	10	04	05	29	08.258	fair
2.449e-01	-8.111e-02	-1.972e-01	1.741e-01	1.624e-02	1.507e-02	2014	10	03	15	27	57.661	good
-2.209e-01	-8.132e-02	-2.190e-02	-1.520e-01	3.521e-02	2.201e-01	2014	10	01	16	56	11.343	good
1.477e-01	-1.175e-01	-1.492e-01	1.577e-01	-3.130e-02	9.546e-02	2014	10	01	08	08	57.998	excellent
-3.263e-02	2.220e-01	-3.373e-01	1.644e-02	7.162e-02	9.879e-03	2014	10	01	10	50	55.107	excellent
-1.038e-01	1.463e-01	-2.541e-01	1.246e-01	-1.332e-02	7.335e-02	2014	10	01	15	01	54.950	excellent
2.306e-03	-1.802e-01	-9.214e-02	2.203e-01	-4.354e-03	9.593e-02	2014	10	02	18	54	03.152	good
1.619e-01	4.200e-02	-2.041e-01	2.158e-01	-2.044e-02	7.759e-02	2014	10	02	06	39	02.998	excellent
-6.570e-02	-1.851e-01	-1.140e-01	1.691e-01	4.183e-02	2.826e-02	2014	10	02	12	39	24.317	good
1.420e-01	-1.373e-01	-1.638e-01	1.721e-01	1.076e-02	5.384e-02	2014	10	02	20	37	06.043	good
-1.365e-01	-1.837e-01	-5.911e-02	1.611e-01	-1.124e-02	9.224e-02	2014	10	05	02	06	16.967	excellent
2.866e-01	-3.707e-02	-1.787e-01	9.263e-02	1.263e-01	2.268e-02	2014	10	05	16	07	32.777	excellent
-2.286e-01	1.607e-01	-7.209e-02	-9.281e-02	8.007e-02	-3.216e-02	2014	10	05	15	55	21.007	good
-1.352e-01	-1.174e-01	-4.098e-02	1.996e-01	-5.345e-02	8.302e-02	2014	10	12	10	12	29	good
-2.211e-01	1.542e-01	4.959e-02	9.042e-02	8.191e-02	7.603e-02	2014	10	12	21	10	23.311	good
-4.882e-01	-1.017e-01	5.620e-02	5.965e-02	-1.844e-03	1.292e-01	2014	10	12	16	37	43.287	excellent

-5.873e-02	-1.252e-01	-2.804e-01	6.116e-02	1.409e-01	6.331e-03	2014	10	13	00	57	06.717	good
2.607e-02	-1.181e-01	-2.888e-01	8.025e-02	1.234e-01	4.154e-02	2014	10	13	04	12	29.126	excellent
-1.162e-01	-1.387e-01	-1.174e-01	1.514e-01	5.536e-02	7.558e-02	2014	10	13	10	22	29.084	excellent
-1.128e-01	-2.729e-02	-2.406e-01	5.661e-02	5.175e-02	3.753e-01	2014	10	14	05	46	13.914	exellent
-5.101e-02	-1.756e-01	-8.505e-02	1.953e-01	1.276e-03	1.195e-01	2014	10	15	15	37	25.945	excellent
-1.267e-01	-1.699e-01	3.343e-02	1.566e-01	-5.422e-02	7.857e-02	2014	10	15	15	03	44.602	excellent
6.492e-02	-9.495e-02	-2.842e-01	6.736e-02	1.452e-01	-3.577e-02	2014	09	30	09	23	48.626	good
-1.426e-01	-1.356e-01	3.347e-03	1.557e-01	-5.829e-02	1.550e-01	2014	10	11	03	29	05.667	good
3.707e-03	3.866e-02	-3.573e-01	5.614e-02	2.090e-01	2.164e-02	2014	10	11	10	53	26.502	good
4.380e-02	2.443e-01	-1.804e-01	4.365e-02	9.993e-02	-2.176e-05	2014	10	07	10	47	20.916	good
2.443e-02	7.095e-02	-2.428e-02	-8.639e-02	-1.620e-01	3.127e-01	2014	10	09	06	24	33.418	excellent
-4.203e-02	-1.463e-01	-3.196e-01	-5.380e-04	1.433e-01	5.826e-02	2014	10	18	23	57	03.695	good
-1.860e-01	8.584e-02	-2.758e-01	1.397e-01	-1.349e-02	6.014e-02	2014	10	19	09	07	50.325	good
2.027e-01	-2.424e-02	-3.047e-01	1.709e-01	-4.330e-02	1.575e-02	2014	10	12	18	33	04.693	moderate
1.319e-01	1.004e-01	-3.874e-01	3.120e-02	9.894e-02	1.908e-02	2014	10	07	06	12	08.593	good
-4.011e-01	-1.326e-01	-3.893e-03	1.173e-01	1.595e-02	6.345e-02	2014	10	16	16	53	27.374	good
7.443e-02	8.687e-02	-6.603e-02	-1.453e-01	-9.859e-02	1.981e-01	2014	10	09	10	16	09.945	moderate
1.913e-01	-1.220e-01	-8.473e-02	1.936e-01	2.385e-02	4.506e-02	2014	09	29	09	57	54.158	excellent
4.999e-02	-1.926e-01	-1.244e-01	1.754e-01	2.482e-02	3.990e-02	2014	09	29	18	03	37.660	excellent
4.020e-02	-1.230e-01	-2.565e-01	1.610e-01	1.968e-02	9.601e-02	2014	10	12	16	47	01.137	excellent
-2.448e-02	-1.879e-01	-1.233e-01	1.689e-01	9.679e-03	1.193e-01	2014	10	05	02	14	37.168	excellent
-8.061e-02	-9.300e-02	-2.670e-01	6.013e-02	1.629e-01	-2.038e-02	2014	10	06	04	02	55.789	good
-2.166e-01	-2.314e-01	4.005e-02	5.036e-02	7.205e-02	3.578e-02	2014	10	02	16	12	35.315	weak
-3.561e-01	1.589e-01	1.186e-01	5.145e-02	2.877e-02	4.702e-02	2014	10	06	06	13	48.626	excellent

Appendix 2: The additional nine moment tensors derived over the reporting week.

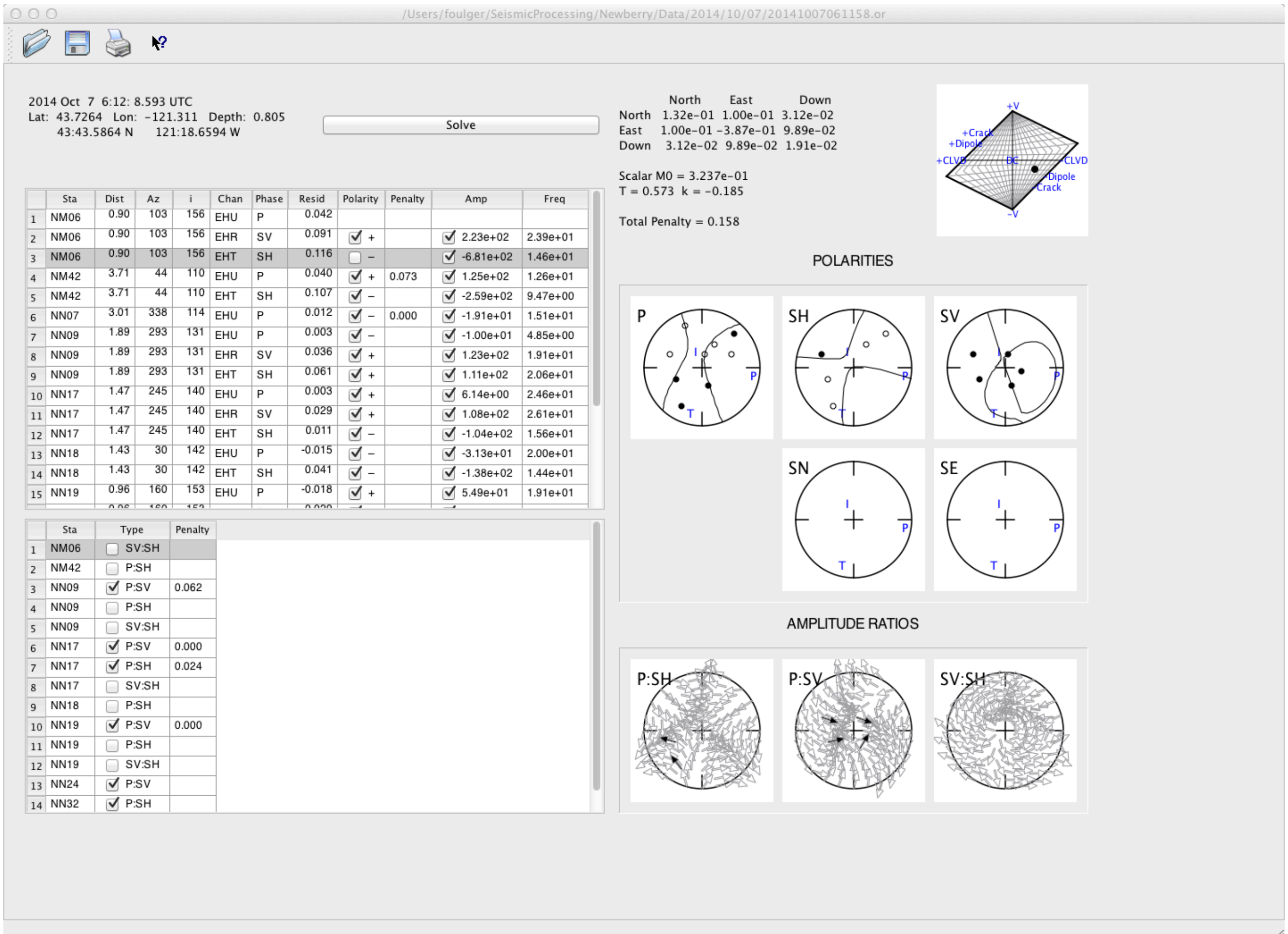
/Users/foulger/SeismicProcessing/Newberry/Data/2014/10/07/20141007061158.or
2014 Oct 7 6:12: 8.593 UTC
Lat: 43.7264 Lon: -121.311 Depth: 0.805
43:43.5864 N 121:18.6594 W
Solve
North East Down
North 1.32e-01 1.00e-01 3.12e-02
East 1.00e-01 -3.87e-01 9.89e-02
Down 3.12e-02 9.89e-02 1.91e-02
Scalar M0 = 3.237e-01
T = 0.573 k = -0.185
Total Penalty = 0.158
+V
+Crack
+Dipole
+CLVD
DC
-CLVD
-Dipole
-Crack
-V
Sta Dist Az i Chan Phase Resid Polarity Penalty Amp Freq
1 NM06 0.90 103 156 EHU P 0.042
2 NM06 0.90 103 156 EHR SV 0.091 + 2.23e+02 2.39e+01
3 NM06 0.90 103 156 EHT SH 0.116 – -6.81e+02 1.46e+01
4 NM42 3.71 44 110 EHU P 0.040 + 0.073 1.25e+02 1.26e+01
5 NM42 3.71 44 110 EHT SH 0.107 – -2.59e+02 9.47e+00
6 NN07 3.01 338 114 EHU P 0.012 – 0.000 -1.91e+01 1.51e+01
7 NN09 1.89 293 131 EHU P 0.003 – -1.00e+01 4.85e+00
8 NN09 1.89 293 131 EHR SV 0.036 + 1.23e+02 1.91e+01
9 NN09 1.89 293 131 EHT SH 0.061 + 1.11e+02 2.06e+01
10 NN17 1.47 245 140 EHU P 0.003 + 6.14e+00 2.46e+01
11 NN17 1.47 245 140 EHR SV 0.029 + 1.08e+02 2.61e+01
12 NN17 1.47 245 140 EHT SH 0.011 – -1.04e+02 1.56e+01
13 NN18 1.43 30 142 EHU P -0.015 – -3.13e+01 2.00e+01
14 NN18 1.43 30 142 EHT SH 0.041 – -1.38e+02 1.44e+01
15 NN19 0.96 160 153 EHU P -0.018 + 5.49e+01 1.91e+01
Sta Type Penalty
1 NM06 SV:SH
2 NM42 P:SH
3 NN09 P:SV 0.062
4 NN09 P:SH
5 NN09 SV:SH
6 NN17 P:SV 0.000
7 NN17 P:SH 0.024
8 NN17 SV:SH
9 NN18 P:SH
10 NN19 P:SV 0.000
11 NN19 P:SH
12 NN19 SV:SH
13 NN24 P:SV
14 NN32 P:SH
POLARITIES
P
SH
SV
SN
SE
AMPLITUDE RATIOS
P:SH
P:SV
SV:SH

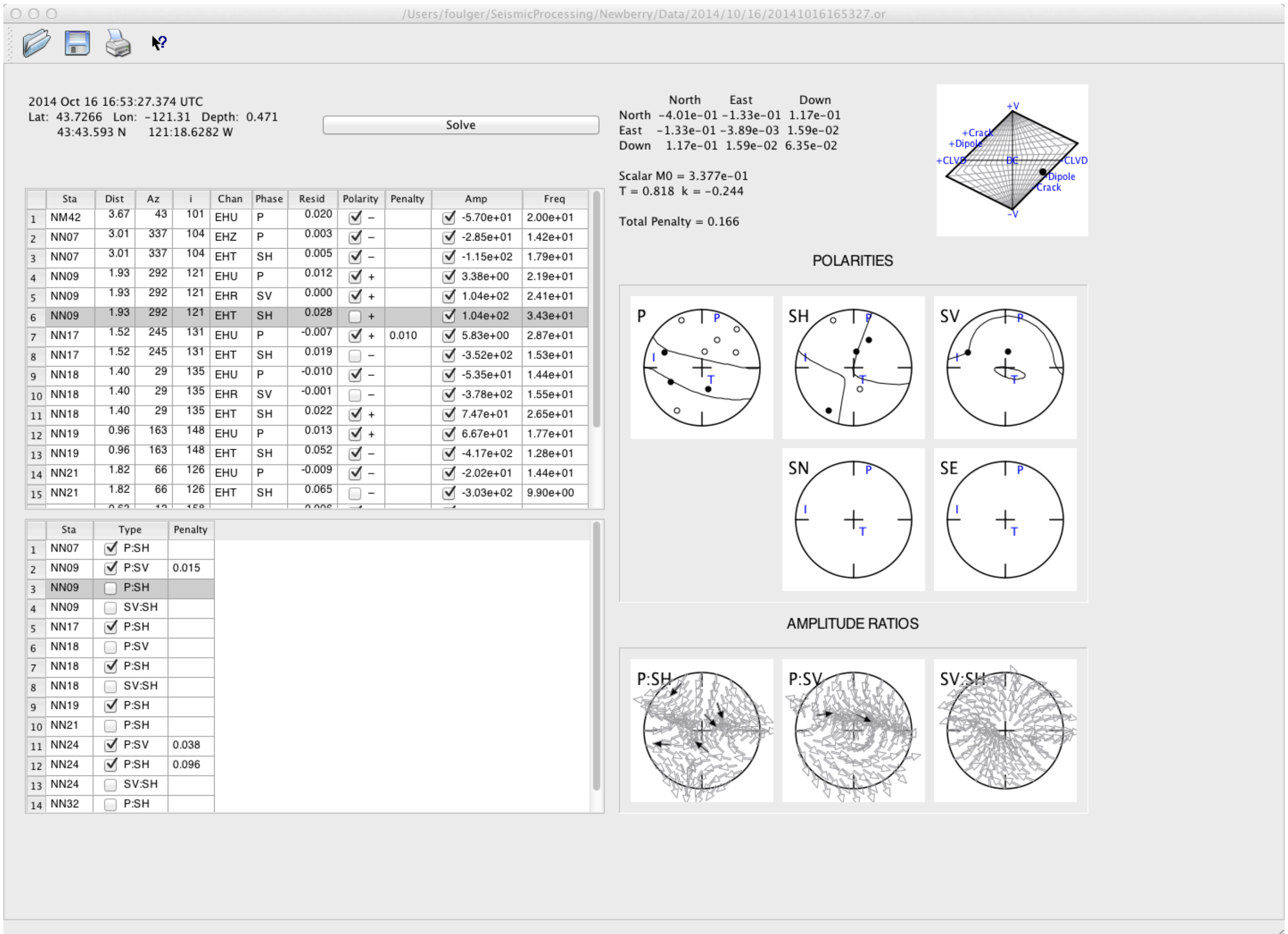
/Users/foulger/SeismicProcessing/Newberry/Data/2014/10/16/20141016165327.or
2014 Oct 16 16:53:27.374 UTC
Lat: 43.7266 Lon: -121.31 Depth: 0.471
43:43.593 N 121:18.6282 W
Solve
Sta Dist Az i Chan Phase Resid Polarity Penalty Amp Freq
1 NM42 3.67 43 101 EHU P 0.020 – -5.70e+01 2.00e+01
2 NN07 3.01 337 104 EHZ P 0.003 – -2.85e+01 1.42e+01
3 NN07 3.01 337 104 EHT SH 0.005 – -1.15e+02 1.79e+01
4 NN09 1.93 292 121 EHU P 0.012 + 3.38e+00 2.19e+01
5 NN09 1.93 292 121 EHR SV 0.000 + 1.04e+02 2.41e+01
6 NN09 1.93 292 121 EHT SH 0.028 + 1.04e+02 3.43e+01
7 NN17 1.52 245 131 EHU P -0.007 + 0.010 5.83e+00 2.87e+01
8 NN17 1.52 245 131 EHT SH 0.019 – -3.52e+02 1.53e+01
9 NN18 1.40 29 135 EHU P -0.010 – -5.35e+01 1.44e+01
10 NN18 1.40 29 135 EHR SV -0.001 – -3.78e+02 1.55e+01
11 NN18 1.40 29 135 EHT SH 0.022 + 7.47e+01 2.65e+01
12 NN19 0.96 163 148 EHU P 0.013 + 6.67e+01 1.77e+01
13 NN19 0.96 163 148 EHT SH 0.052 – -4.17e+02 1.28e+01
14 NN21 1.82 66 126 EHU P -0.009 – -2.02e+01 1.44e+01
15 NN21 1.82 66 126 EHT SH 0.065 – -3.03e+02 9.90e+00
Sta Type Penalty
1 NN07 P:SH
2 NN09 P:SV 0.015
3 NN09 P:SH
4 NN09 SV:SH
5 NN17 P:SH
6 NN18 P:SV
7 NN18 P:SH
8 NN18 SV:SH
9 NN19 P:SH
10 NN21 P:SH
11 NN24 P:SV 0.038
12 NN24 P:SH 0.096
13 NN24 SV:SH
14 NN32 P:SH
North East Down
North -4.01e-01 -1.33e-01 1.17e-01
East -1.33e-01 -3.89e-03 1.59e-02
Down 1.17e-01 1.59e-02 6.35e-02
Scalar M0 = 3.377e-01
T = 0.818 k = -0.244
Total Penalty = 0.166
+V
+Crack
+Dipole
+CLVD
DC
-CLVD
-Dipole
-Crack
-V
POLARITIES
P
SH
SV
SN
SE
AMPLITUDE RATIOS
P:SH
P:SV
SV:SH

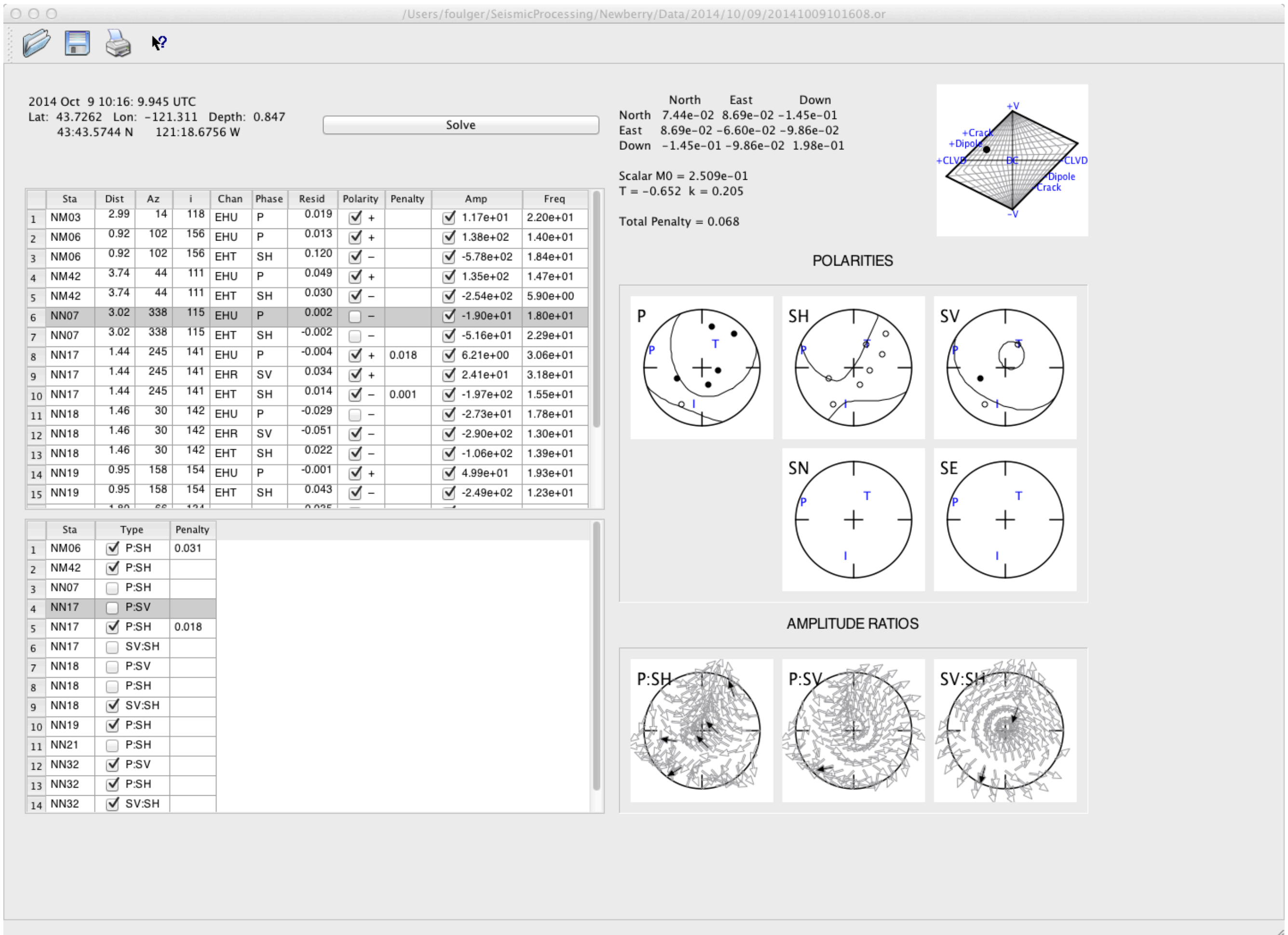
/Users/foulger/SeismicProcessing/Newberry/Data/2014/10/09/20141009101608.or
2014 Oct 9 10:16: 9.945 UTC
Lat: 43.7262 Lon: -121.311 Depth: 0.847
43:43.5744 N 121:18.6756 W
Solve
North East Down
North 7.44e-02 8.69e-02 -1.45e-01
East 8.69e-02 -6.60e-02 -9.86e-02
Down -1.45e-01 -9.86e-02 1.98e-01
Scalar M0 = 2.509e-01
T = -0.652 k = 0.205
Total Penalty = 0.068
+V
+Crack
+Dipole
+CLVD
DC
CLVD
Dipole
Crack
-V
Sta Dist Az i Chan Phase Resid Polarity Penalty Amp Freq
1 NM03 2.99 14 118 EHU P 0.019 + 1.17e+01 2.20e+01
2 NM06 0.92 102 156 EHU P 0.013 + 1.38e+02 1.40e+01
3 NM06 0.92 102 156 EHT SH 0.120 – -5.78e+02 1.84e+01
4 NM42 3.74 44 111 EHU P 0.049 + 1.35e+02 1.47e+01
5 NM42 3.74 44 111 EHT SH 0.030 – -2.54e+02 5.90e+00
6 NN07 3.02 338 115 EHU P 0.002 – -1.90e+01 1.80e+01
7 NN07 3.02 338 115 EHT SH -0.002 – -5.16e+01 2.29e+01
8 NN17 1.44 245 141 EHU P -0.004 + 0.018 6.21e+00 3.06e+01
9 NN17 1.44 245 141 EHR SV 0.034 + 2.41e+01 3.18e+01
10 NN17 1.44 245 141 EHT SH 0.014 – 0.001 -1.97e+02 1.55e+01
11 NN18 1.46 30 142 EHU P -0.029 – -2.73e+01 1.78e+01
12 NN18 1.46 30 142 EHR SV -0.051 – -2.90e+02 1.30e+01
13 NN18 1.46 30 142 EHT SH 0.022 – -1.06e+02 1.39e+01
14 NN19 0.95 158 154 EHU P -0.001 + 4.99e+01 1.93e+01
15 NN19 0.95 158 154 EHT SH 0.043 – -2.49e+02 1.23e+01
Sta Type Penalty
1 NM06 P:SH 0.031
2 NM42 P:SH
3 NN07 P:SH
4 NN17 P:SV
5 NN17 P:SH 0.018
6 NN17 SV:SH
7 NN18 P:SV
8 NN18 P:SH
9 NN18 SV:SH
10 NN19 P:SH
11 NN21 P:SH
12 NN32 P:SV
13 NN32 P:SH
14 NN32 SV:SH
POLARITIES
P
SH
SV
SN
SE
AMPLITUDE RATIOS
P:SH
P:SV
SV:SH

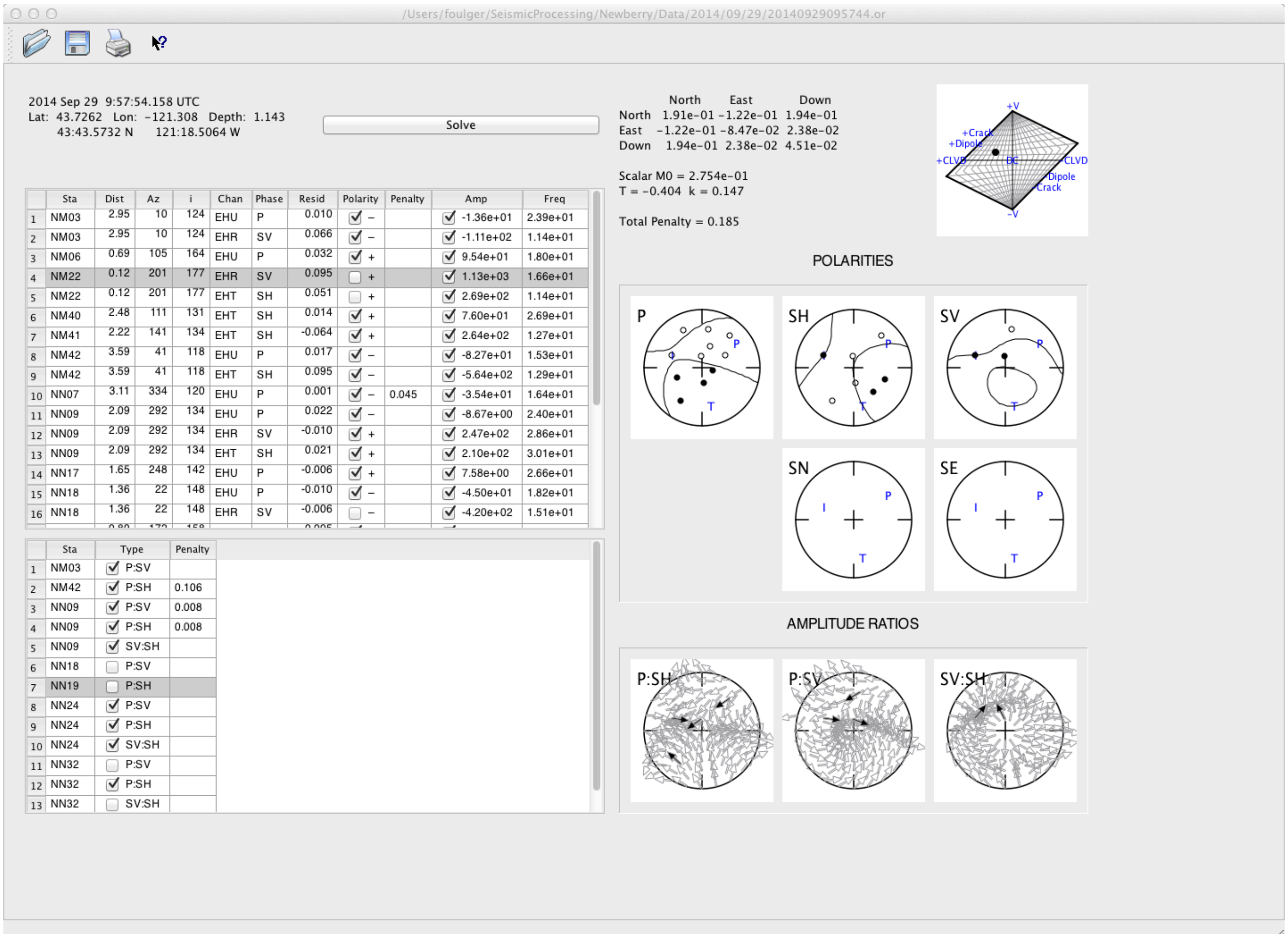
/Users/foulger/SeismicProcessing/Newberry/Data/2014/09/29/20140929095744.or
2014 Sep 29 9:57:54.158 UTC
Lat: 43.7262 Lon: −121.308 Depth: 1.143
43:43.5732 N 121:18.5064 W
Solve
Sta Dist Az i Chan Phase Resid Polarity Penalty Amp Freq
1 NM03 2.95 10 124 EHU P 0.010 [x] − [x] -1.36e+01 2.39e+01
2 NM03 2.95 10 124 EHR SV 0.066 [x] − [x] -1.11e+02 1.14e+01
3 NM06 0.69 105 164 EHU P 0.032 [x] + [x] 9.54e+01 1.80e+01
4 NM22 0.12 201 177 EHR SV 0.095 [ ] + [x] 1.13e+03 1.66e+01
5 NM22 0.12 201 177 EHT SH 0.051 [ ] + [x] 2.69e+02 1.14e+01
6 NM40 2.48 111 131 EHT SH 0.014 [x] + [x] 7.60e+01 2.69e+01
7 NM41 2.22 141 134 EHT SH -0.064 [x] + [x] 2.64e+02 1.27e+01
8 NM42 3.59 41 118 EHU P 0.017 [x] − [x] -8.27e+01 1.53e+01
9 NM42 3.59 41 118 EHT SH 0.095 [x] − [x] -5.64e+02 1.29e+01
10 NN07 3.11 334 120 EHU P 0.001 [x] − 0.045 [x] -3.54e+01 1.64e+01
11 NN09 2.09 292 134 EHU P 0.022 [x] − [x] -8.67e+00 2.40e+01
12 NN09 2.09 292 134 EHR SV -0.010 [x] + [x] 2.47e+02 2.86e+01
13 NN09 2.09 292 134 EHT SH 0.021 [x] + [x] 2.10e+02 3.01e+01
14 NN17 1.65 248 142 EHU P -0.006 [x] + [x] 7.58e+00 2.66e+01
15 NN18 1.36 22 148 EHU P -0.010 [x] − [x] -4.50e+01 1.82e+01
16 NN18 1.36 22 148 EHR SV -0.006 [ ] − [x] -4.20e+02 1.51e+01
Sta Type Penalty
1 NM03 [x] P:SV
2 NM42 [x] P:SH 0.106
3 NN09 [x] P:SV 0.008
4 NN09 [x] P:SH 0.008
5 NN09 [x] SV:SH
6 NN18 [ ] P:SV
7 NN19 [ ] P:SH
8 NN24 [x] P:SV
9 NN24 [x] P:SH
10 NN24 [x] SV:SH
11 NN32 [ ] P:SV
12 NN32 [x] P:SH
13 NN32 [ ] SV:SH
North East Down
North 1.91e−01 −1.22e−01 1.94e−01
East −1.22e−01 −8.47e−02 2.38e−02
Down 1.94e−01 2.38e−02 4.51e−02
Scalar M0 = 2.754e−01
T = −0.404 k = 0.147
Total Penalty = 0.185
+V
+Crack
+Dipole
+CLVD
DC
−CLVD
−Dipole
−Crack
−V
POLARITIES
P
SH
SV
SN
SE
AMPLITUDE RATIOS
P:SH
P:SV
SV:SH

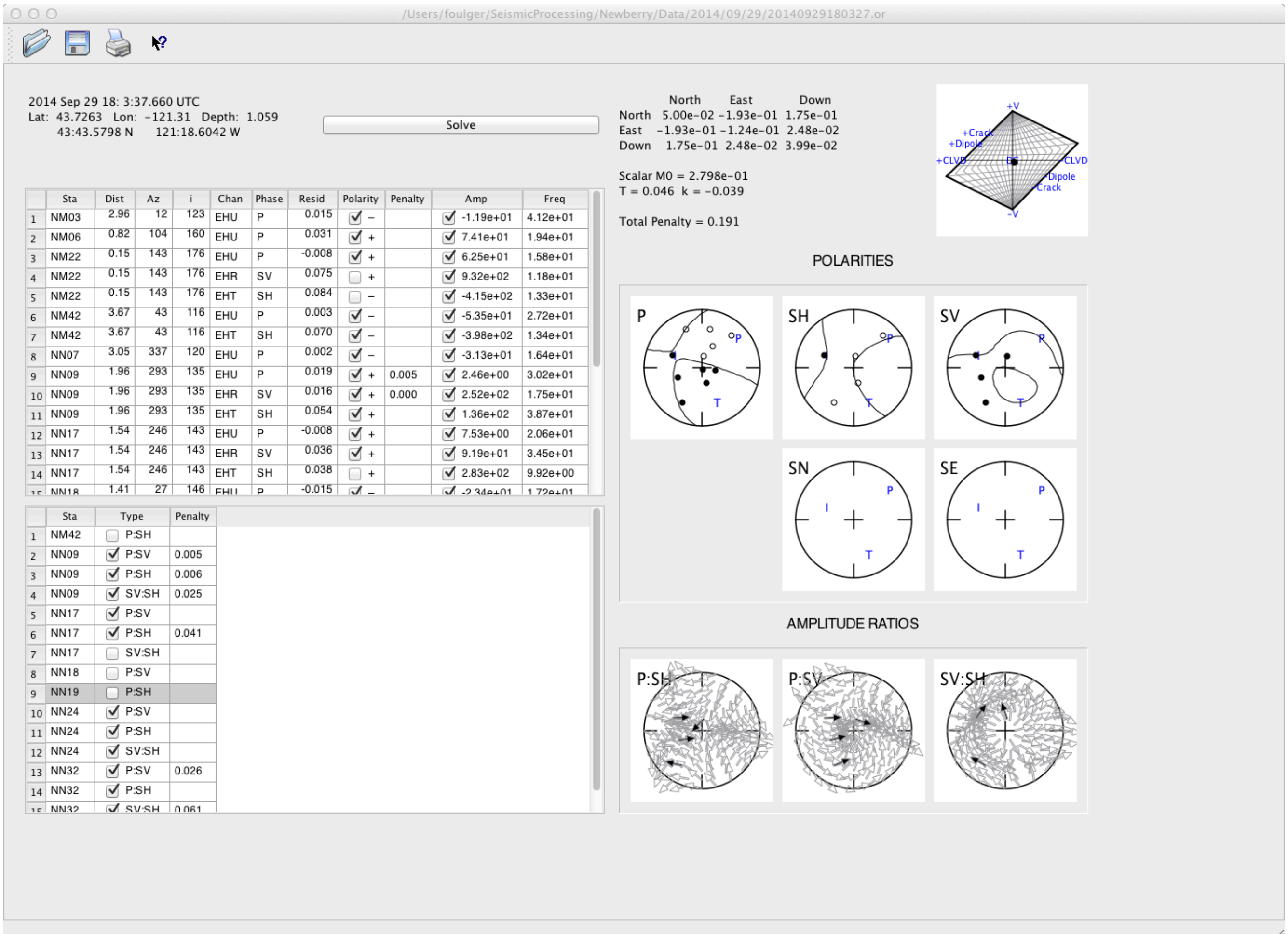
/Users/foulger/SeismicProcessing/Newberry/Data/2014/09/29/20140929180327.or
2014 Sep 29 18: 3:37.660 UTC
Lat: 43.7263 Lon: -121.31 Depth: 1.059
43:43.5798 N 121:18.6042 W
Solve
North East Down
North 5.00e-02 -1.93e-01 1.75e-01
East -1.93e-01 -1.24e-01 2.48e-02
Down 1.75e-01 2.48e-02 3.99e-02
Scalar M0 = 2.798e-01
T = 0.046 k = -0.039
Total Penalty = 0.191
+V
+Crack
+Dipole
+CLVD
CLVD
Dipole
Crack
-V
Sta Dist Az i Chan Phase Resid Polarity Penalty Amp Freq
1 NM03 2.96 12 123 EHU P 0.015 – -1.19e+01 4.12e+01
2 NM06 0.82 104 160 EHU P 0.031 + 7.41e+01 1.94e+01
3 NM22 0.15 143 176 EHU P -0.008 + 6.25e+01 1.58e+01
4 NM22 0.15 143 176 EHR SV 0.075 + 9.32e+02 1.18e+01
5 NM22 0.15 143 176 EHT SH 0.084 – -4.15e+02 1.33e+01
6 NM42 3.67 43 116 EHU P 0.003 – -5.35e+01 2.72e+01
7 NM42 3.67 43 116 EHT SH 0.070 – -3.98e+02 1.34e+01
8 NN07 3.05 337 120 EHU P 0.002 – -3.13e+01 1.64e+01
9 NN09 1.96 293 135 EHU P 0.019 + 0.005 2.46e+00 3.02e+01
10 NN09 1.96 293 135 EHR SV 0.016 + 0.000 2.52e+02 1.75e+01
11 NN09 1.96 293 135 EHT SH 0.054 + 1.36e+02 3.87e+01
12 NN17 1.54 246 143 EHU P -0.008 + 7.53e+00 2.06e+01
13 NN17 1.54 246 143 EHR SV 0.036 + 9.19e+01 3.45e+01
14 NN17 1.54 246 143 EHT SH 0.038 + 2.83e+02 9.92e+00
Sta Type Penalty
1 NM42 P:SH
2 NN09 P:SV 0.005
3 NN09 P:SH 0.006
4 NN09 SV:SH 0.025
5 NN17 P:SV
6 NN17 P:SH 0.041
7 NN17 SV:SH
8 NN18 P:SV
9 NN19 P:SH
10 NN24 P:SV
11 NN24 P:SH
12 NN24 SV:SH
13 NN32 P:SV 0.026
14 NN32 P:SH
POLARITIES
P
SH
SV
SN
SE
AMPLITUDE RATIOS
P:SH
P:SV
SV:SH

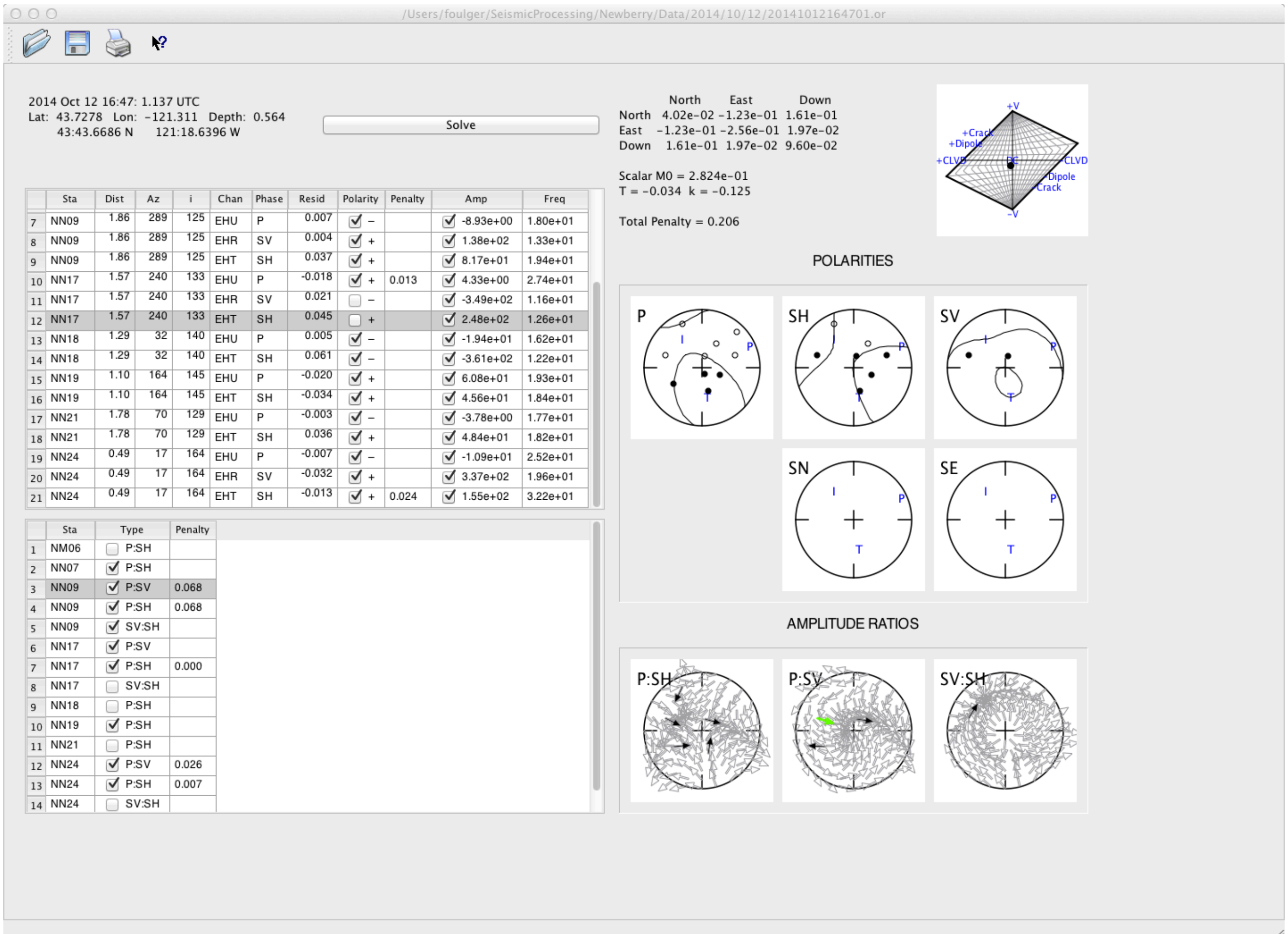

2014 Oct 12 16:47: 1.137 UTC
Lat: 43.7278 Lon: -121.311 Depth: 0.564
43:43.6686 N 121:18.6396 W

	North	East	Down
North	4.02e-02	-1.23e-01	1.61e-01
East	-1.23e-01	-2.56e-01	1.97e-02
Down	1.61e-01	1.97e-02	9.60e-02

Scalar M0 = 2.824e-01
T = -0.034 k = -0.125

Total Penalty = 0.206

	Sta	Dist	Az	i	Chan	Phase	Resid	Polarity	Penalty	Amp	Freq
7	NN09	1.86	289	125	EHU	P	0.007	✓ –		✓ -8.93e+00	1.80e+01
8	NN09	1.86	289	125	EHR	SV	0.004	✓ +		✓ 1.38e+02	1.33e+01
9	NN09	1.86	289	125	EHT	SH	0.037	✓ +		✓ 8.17e+01	1.94e+01
10	NN17	1.57	240	133	EHU	P	-0.018	✓ +	0.013	✓ 4.33e+00	2.74e+01
11	NN17	1.57	240	133	EHR	SV	0.021	–		✓ -3.49e+02	1.16e+01
12	NN17	1.57	240	133	EHT	SH	0.045	+		✓ 2.48e+02	1.26e+01
13	NN18	1.29	32	140	EHU	P	0.005	✓ –		✓ -1.94e+01	1.62e+01
14	NN18	1.29	32	140	EHT	SH	0.061	✓ –		✓ -3.61e+02	1.22e+01
15	NN19	1.10	164	145	EHU	P	-0.020	✓ +		✓ 6.08e+01	1.93e+01
16	NN19	1.10	164	145	EHT	SH	-0.034	✓ +		✓ 4.56e+01	1.84e+01
17	NN21	1.78	70	129	EHU	P	-0.003	✓ –		✓ -3.78e+00	1.77e+01
18	NN21	1.78	70	129	EHT	SH	0.036	✓ +		✓ 4.84e+01	1.82e+01
19	NN24	0.49	17	164	EHU	P	-0.007	✓ –		✓ -1.09e+01	2.52e+01
20	NN24	0.49	17	164	EHR	SV	-0.032	✓ +		✓ 3.37e+02	1.96e+01
21	NN24	0.49	17	164	EHT	SH	-0.013	✓ +	0.024	✓ 1.55e+02	3.22e+01

	Sta	Type	Penalty
1	NM06	P:SH	
2	NN07	✓ P:SH	
3	NN09	✓ P:SV	0.068
4	NN09	✓ P:SH	0.068
5	NN09	✓ SV:SH	
6	NN17	✓ P:SV	
7	NN17	✓ P:SH	0.000
8	NN17	SV:SH	
9	NN18	P:SH	
10	NN19	✓ P:SH	
11	NN21	P:SH	
12	NN24	✓ P:SV	0.026
13	NN24	✓ P:SH	0.007
14	NN24	SV:SH	

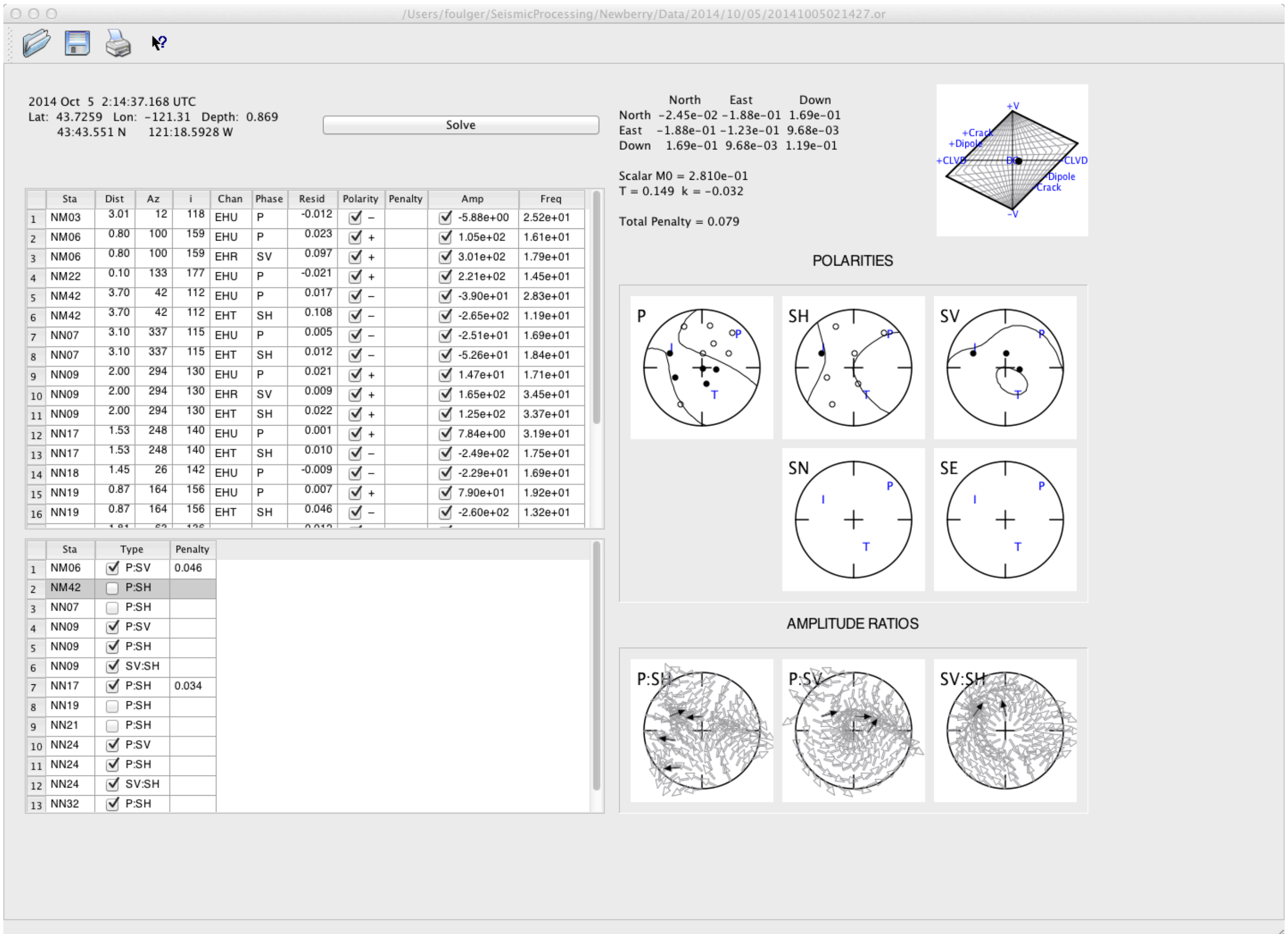
/Users/foulger/SeismicProcessing/Newberry/Data/2014/10/05/20141005021427.or
2014 Oct 5 2:14:37.168 UTC
Lat: 43.7259 Lon: -121.31 Depth: 0.869
43:43.551 N 121:18.5928 W
Solve
North East Down
North -2.45e-02 -1.88e-01 1.69e-01
East -1.88e-01 -1.23e-01 9.68e-03
Down 1.69e-01 9.68e-03 1.19e-01
Scalar M0 = 2.810e-01
T = 0.149 k = -0.032
Total Penalty = 0.079
+V
+Crack
+Dipole
+CLVD
-CLVD
-Dipole
-Crack
-V
Sta Dist Az i Chan Phase Resid Polarity Penalty Amp Freq
1 NM03 3.01 12 118 EHU P -0.012 – -5.88e+00 2.52e+01
2 NM06 0.80 100 159 EHU P 0.023 + 1.05e+02 1.61e+01
3 NM06 0.80 100 159 EHR SV 0.097 + 3.01e+02 1.79e+01
4 NM22 0.10 133 177 EHU P -0.021 + 2.21e+02 1.45e+01
5 NM42 3.70 42 112 EHU P 0.017 – -3.90e+01 2.83e+01
6 NM42 3.70 42 112 EHT SH 0.108 – -2.65e+02 1.19e+01
7 NN07 3.10 337 115 EHU P 0.005 – -2.51e+01 1.69e+01
8 NN07 3.10 337 115 EHT SH 0.012 – -5.26e+01 1.84e+01
9 NN09 2.00 294 130 EHU P 0.021 + 1.47e+01 1.71e+01
10 NN09 2.00 294 130 EHR SV 0.009 + 1.65e+02 3.45e+01
11 NN09 2.00 294 130 EHT SH 0.022 + 1.25e+02 3.37e+01
12 NN17 1.53 248 140 EHU P 0.001 + 7.84e+00 3.19e+01
13 NN17 1.53 248 140 EHT SH 0.010 – -2.49e+02 1.75e+01
14 NN18 1.45 26 142 EHU P -0.009 – -2.29e+01 1.69e+01
15 NN19 0.87 164 156 EHU P 0.007 + 7.90e+01 1.92e+01
16 NN19 0.87 164 156 EHT SH 0.046 – -2.60e+02 1.32e+01
Sta Type Penalty
1 NM06 P:SV 0.046
2 NM42 P:SH
3 NN07 P:SH
4 NN09 P:SV
5 NN09 P:SH
6 NN09 SV:SH
7 NN17 P:SH 0.034
8 NN19 P:SH
9 NN21 P:SH
10 NN24 P:SV
11 NN24 P:SH
12 NN24 SV:SH
13 NN32 P:SH
POLARITIES
P
SH
SV
SN
SE
AMPLITUDE RATIOS
P:SH
P:SV
SV:SH

/Users/foulger/SeismicProcessing/Newberry/Data/2014/10/06/20141006040245.or

2014 Oct 6 4: 2:55.789 UTC
Lat: 43.7273 Lon: -121.309 Depth: 0.662
43:43.6398 N 121:18.537 W

Solve

	Sta	Dist	Az	i	Chan	Phase	Resid	Polarity	Penalty	Amp	Freq
1	NM03	2.83	11	115	EHU	P	0.048	☐ +		☑ 4.31e+00	2.39e+01
2	NM22	0.23	180	173	EHT	SH	0.060	☑ +		☑ 3.68e+02	1.38e+01
3	NN07	2.98	334	111	EHU	P	0.011	☑ –		☑ -8.70e+00	1.59e+01
4	NN07	2.98	334	111	EHR	SV	-0.022	☑ +		☑ 3.17e+01	1.68e+01
5	NN09	2.01	289	125	EHU	P	0.010	☑ –		☑ -1.94e+00	2.66e+01
6	NN09	2.01	289	125	EHR	SV	0.011	☑ +		☑ 6.38e+01	2.46e+01
7	NN09	2.01	289	125	EHT	SH	0.039	☑ +		☑ 6.60e+01	2.09e+01
8	NN17	1.66	244	133	EHU	P	-0.022	☑ +		☑ 4.25e+00	2.58e+01
9	NN17	1.66	244	133	EHR	SV	0.000	☑ +		☑ 1.34e+02	2.08e+01
10	NN17	1.66	244	133	EHT	SH	0.020	☑ +		☑ 2.64e+02	1.16e+01
11	NN18	1.27	26	143	EHU	P	0.007	☑ –		☑ -2.07e+01	1.77e+01
12	NN18	1.27	26	143	EHT	SH	0.091	☑ –		☑ -8.42e+01	1.54e+01
13	NN19	1.01	171	149	EHU	P	-0.014	☑ +		☑ 3.25e+01	1.84e+01
14	NN19	1.01	171	149	EHR	SV	-0.016	☑ –		☑ -8.27e+01	2.07e+01
15	NN19	1.01	171	149	EHT	SH	0.021	☑ +		☑ 6.10e+01	2.51e+01

	Sta	Type	Penalty
1	NN07	☑ P:SV	0.004
2	NN09	☑ P:SV	0.008
3	NN09	☐ P:SH	
4	NN09	☐ SV:SH	
5	NN17	☑ P:SV	0.021
6	NN17	☑ P:SH	
7	NN17	☐ SV:SH	
8	NN18	☑ P:SH	
9	NN19	☑ P:SV	
10	NN19	☐ P:SH	
11	NN19	☐ SV:SH	
12	NN24	☑ P:SV	0.006
13	NN24	☐ P:SH	
14	NN24	☐ SV:SH	

	North	East	Down
North	-8.06e-02	-9.30e-02	6.01e-02
East	-9.30e-02	-2.67e-01	1.63e-01
Down	6.01e-02	1.63e-01	-2.04e-02

Scalar M0 = 2.791e-01
T = 0.606 k = -0.317

Total Penalty = 0.039

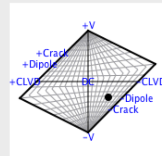

POLARITIES

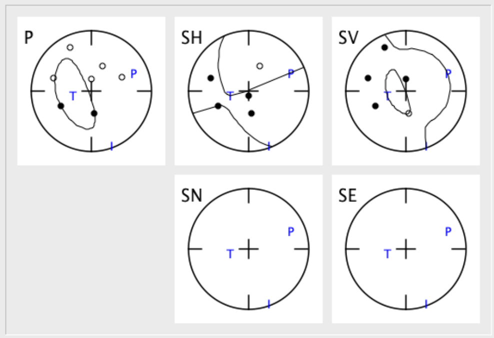

AMPLITUDE RATIOS

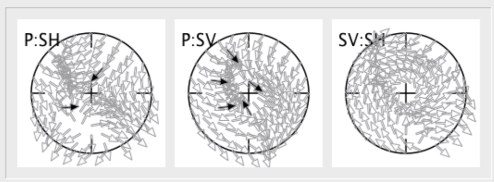

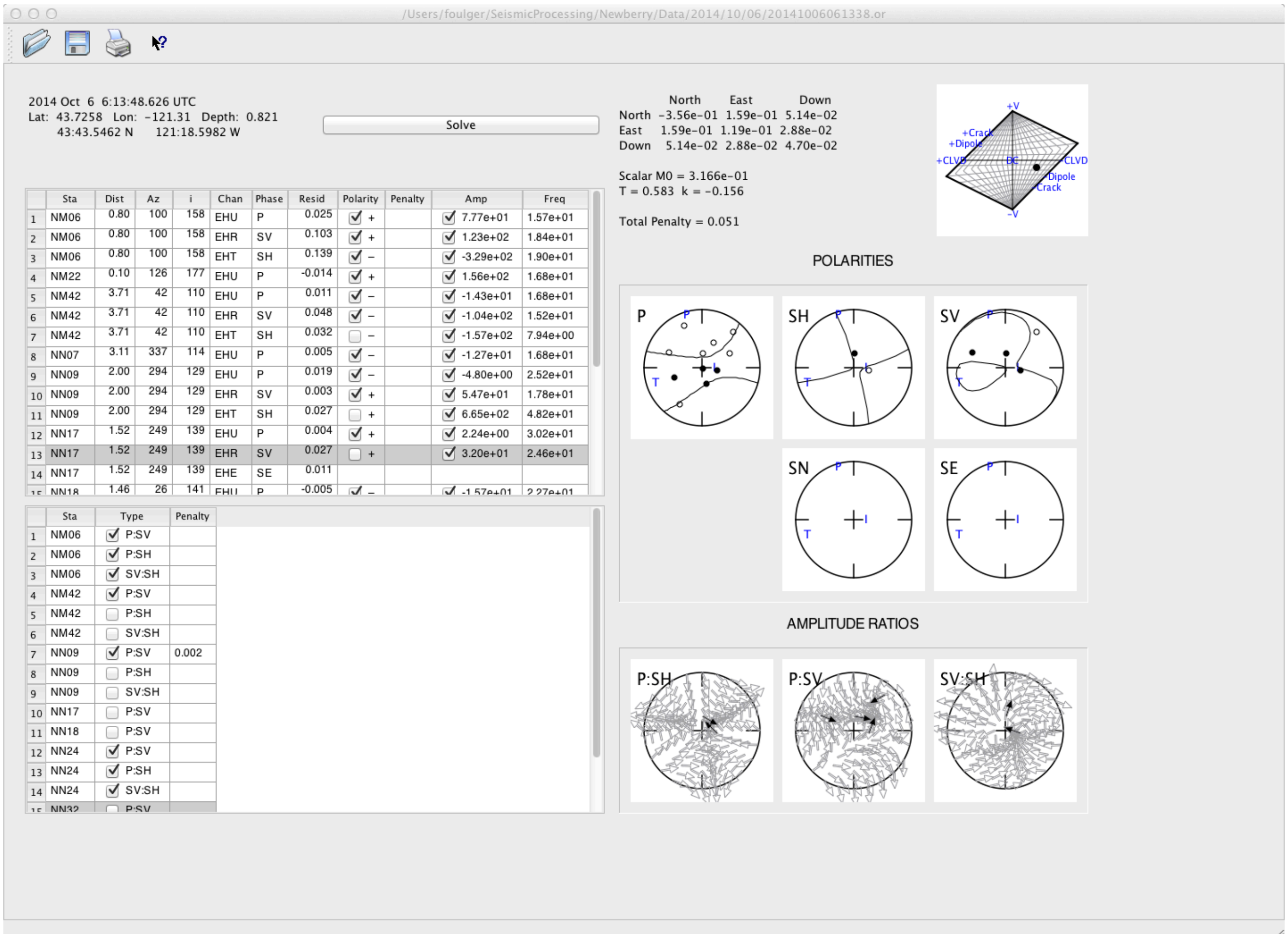
/Users/foulger/SeismicProcessing/Newberry/Data/2014/10/06/20141006061338.or
2014 Oct 6 6:13:48.626 UTC
Lat: 43.7258 Lon: -121.31 Depth: 0.821
43:43.5462 N 121:18.5982 W
Solve
North East Down
North -3.56e-01 1.59e-01 5.14e-02
East 1.59e-01 1.19e-01 2.88e-02
Down 5.14e-02 2.88e-02 4.70e-02
Scalar M0 = 3.166e-01
T = 0.583 k = -0.156
Total Penalty = 0.051
+V
+Crack
+Dipole
+CLVD
DC
CLVD
Dipole
Crack
-V
Sta Dist Az i Chan Phase Resid Polarity Penalty Amp Freq
1 NM06 0.80 100 158 EHU P 0.025 + 7.77e+01 1.57e+01
2 NM06 0.80 100 158 EHR SV 0.103 + 1.23e+02 1.84e+01
3 NM06 0.80 100 158 EHT SH 0.139 – -3.29e+02 1.90e+01
4 NM22 0.10 126 177 EHU P -0.014 + 1.56e+02 1.68e+01
5 NM42 3.71 42 110 EHU P 0.011 – -1.43e+01 1.68e+01
6 NM42 3.71 42 110 EHR SV 0.048 – -1.04e+02 1.52e+01
7 NM42 3.71 42 110 EHT SH 0.032 – -1.57e+02 7.94e+00
8 NN07 3.11 337 114 EHU P 0.005 – -1.27e+01 1.68e+01
9 NN09 2.00 294 129 EHU P 0.019 – -4.80e+00 2.52e+01
10 NN09 2.00 294 129 EHR SV 0.003 + 5.47e+01 1.78e+01
11 NN09 2.00 294 129 EHT SH 0.027 + 6.65e+02 4.82e+01
12 NN17 1.52 249 139 EHU P 0.004 + 2.24e+00 3.02e+01
13 NN17 1.52 249 139 EHR SV 0.027 + 3.20e+01 2.46e+01
14 NN17 1.52 249 139 EHE SE 0.011
Sta Type Penalty
1 NM06 P:SV
2 NM06 P:SH
3 NM06 SV:SH
4 NM42 P:SV
5 NM42 P:SH
6 NM42 SV:SH
7 NN09 P:SV 0.002
8 NN09 P:SH
9 NN09 SV:SH
10 NN17 P:SV
11 NN18 P:SV
12 NN24 P:SV
13 NN24 P:SH
14 NN24 SV:SH
POLARITIES
P
SH
SV
SN
SE
AMPLITUDE RATIOS
P:SH
P:SV
SV:SH

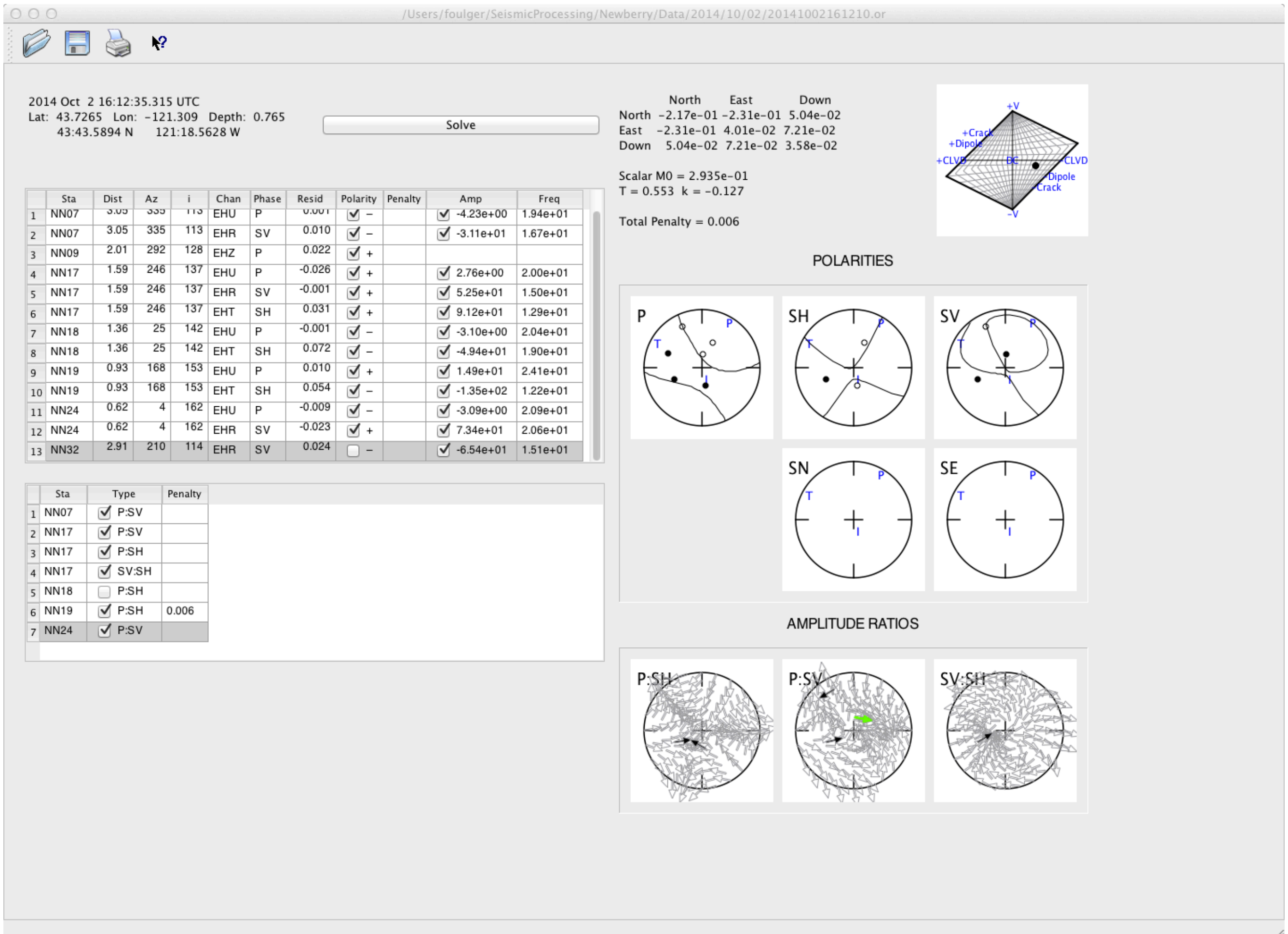

	Sta	Dist	Az	i	Chan	Phase	Resid	Polarity	Penalty	Amp	Freq
1	NN07	3.05	335	113	EHU	P	0.001	✓ –		✓ -4.23e+00	1.94e+01
2	NN07	3.05	335	113	EHR	SV	0.010	✓ –		✓ -3.11e+01	1.67e+01
3	NN09	2.01	292	128	EHZ	P	0.022	✓ +			
4	NN17	1.59	246	137	EHU	P	-0.026	✓ +		✓ 2.76e+00	2.00e+01
5	NN17	1.59	246	137	EHR	SV	-0.001	✓ +		✓ 5.25e+01	1.50e+01
6	NN17	1.59	246	137	EHT	SH	0.031	✓ +		✓ 9.12e+01	1.29e+01
7	NN18	1.36	25	142	EHU	P	-0.001	✓ –		✓ -3.10e+00	2.04e+01
8	NN18	1.36	25	142	EHT	SH	0.072	✓ –		✓ -4.94e+01	1.90e+01
9	NN19	0.93	168	153	EHU	P	0.010	✓ +		✓ 1.49e+01	2.41e+01
10	NN19	0.93	168	153	EHT	SH	0.054	✓ –		✓ -1.35e+02	1.22e+01
11	NN24	0.62	4	162	EHU	P	-0.009	✓ –		✓ -3.09e+00	2.09e+01
12	NN24	0.62	4	162	EHR	SV	-0.023	✓ +		✓ 7.34e+01	2.06e+01
13	NN32	2.91	210	114	EHR	SV	0.024	☐ –		✓ -6.54e+01	1.51e+01

	Sta	Type	Penalty
1	NN07	✓ P:SV	
2	NN17	✓ P:SV	
3	NN17	✓ P:SH	
4	NN17	✓ SV:SH	
5	NN18	☐ P:SH	
6	NN19	✓ P:SH	0.006
7	NN24	✓ P:SV	